# IoT Integration of a Voltage Controlled Active Magnetic Bearing for Real-Time Remote Monitoring and Control.

by

Nyandieka H. Aboki

Submitted in Partial Fulfillment of the Requirements

for the Degree of

Master of Science in Engineering

in the

Mechanical Engineering

Program

YOUNGSTOWN STATE UNIVERSITY

December 2023

IoT Integration of a Voltage Controlled Active Magnetic Bearing for Real Time Remote Monitoring and Control.

Nyandieka H. Aboki

I hereby release this thesis to the public. I understand that this thesis will be made available from the OhioLINK ETD Center and the Maag Library Circulation Desk for public access. I also authorize the University or other individuals to make copies of this thesis as needed for scholarly research.

Signature:

---

*Nyandieka H. Aboki*, Student Date

Approvals:

---

*Dr. Alexander H. Pesch*, Thesis Advisor Date

---

Dr. *Kyosung Choo*, Committee Member Date

---

Dr. *Jae Joong Ryu*, Committee Member Date

---

Dr. Salvatore A. Sanders, Dean of Graduate Studies Date

# ABSTRACT

This thesis contributes to the development of a voltage controlled active magnetic bearing by using transistors to perform the switching action which eventually controls the position of a rotor. The research further presents a new architecture of integrating Active Magnetic Bearings (AMBs) to the Internet for real time remote monitoring and control. The architecture involved the integration of AMB sensors to an IoT gateway via an ADC. ThingSpeak cloud service platform was used to connect the IoT gateway to the cloud using the HTTP protocol enabling the access of the real time data from the AMB sensors remotely.

Furthermore, to control the AMB remotely, a program was developed that sends signals from a remote computer to the IoT gateway which is triggered to send a command signal to the AMB controller to control the AMB. To demonstrate the success control of the AMB, a remote step response was successfully performed. The step response was compared to a local step response to evaluate how the AMB response match irrespective of the mode of operation. The closely matching response provided the confidence of operating an AMB remotely from anywhere around the world to perform corrective actions whenever a common fault such as misalignment and imbalance are detected.

The research further compared GaNTs and MOSFETs performance under active levitation of the AMB. It was established that better control and stability is achieved when using GaNTs for switching action as compared to MOSFETs. This was due to the wide bandgap characteristic of the GaN transistors and higher switching frequencies.

# TABLE OF CONTENTS

# NOMENCLATURE

AMB: Active Magnetic Bearing

PWM: Pulse Width Modulation

GUI: Graphical User Interface

IoT: Internet of Things

IIoT: Industrial Internet of Things

PLC: Programmable Logic Controller

SCADA: supervisory Control and Data Acquisition

IPv6: Internet Protocol Version 6

SISO: single Input, Single Output

GaN: Gallium Nitride

MOSFET: Metal-Oxide Semiconductor field-effect-transistor

PID: Proportional-Integral-Derivative

ADC: Analog-Digital-Converter

LTI: Linear Time Invariant

$I^2C$: Inter-Integrated Circuit

SPI:  Serial Peripheral Interface

UART:  Universal Asynchronous Receiver/Transmitter

RFID:  Radio Frequency Identification

NFC:  Near Field Communication

HTTP: Hypertext Transfer Protocol

MQTT: Message Queuing Telemetry Transport

CoAP: Constrained Application Protocol

XMPP: Extensible Messaging and Presence Protocol

TCP: Transmission Control Protocol

BLE: Bluetooth Low Energy

GPIO: General Purpose Input/Output

VNC: Virtual Network Computing

SSH: Secure Shell

FFT: Fast Fourier Transform

SCL: Serial Clock Line

SDA: Serial Data Line

# LIST OF TABLES

# LIST OF FIGURES

# 1 INTRODUCTION

Active magnetic bearings are mechatronics devices that generate magnetic field force using the principle of electromagnetism to support a rotor or shaft in a predetermined position relative to a stator [[1]. The magnetic field forces generated are actively controlled by a controller. There is no physical contact between the stator and the rotor. Active magnetic bearings have a position sensor that checks the position of the rotor, and the instantaneous position is compared with the reference set point [2]. Any deviations from the reference position prompt the controller to generate a control signal. In Fig 1.1, the general layout of an active magnetic bearing is shown [3].

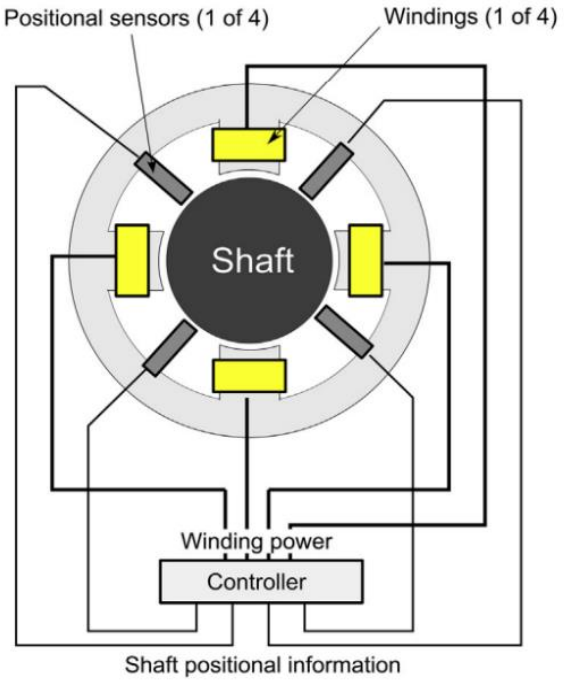


*Fig 1.1. A radial magnetic bearing showing the control system and position sensors* [3].

There are two control architectures that are employed by active magnetic bearing. One of the architectures takes the control signal and changes the signal into a control current using power amplifiers. The control current then actuates the electromagnets to produce a magnetic field force. The magnitude of the magnetic field force is such that it provides sufficient support for the rotor to maintain its set position as shown in Fig 1.2) a.

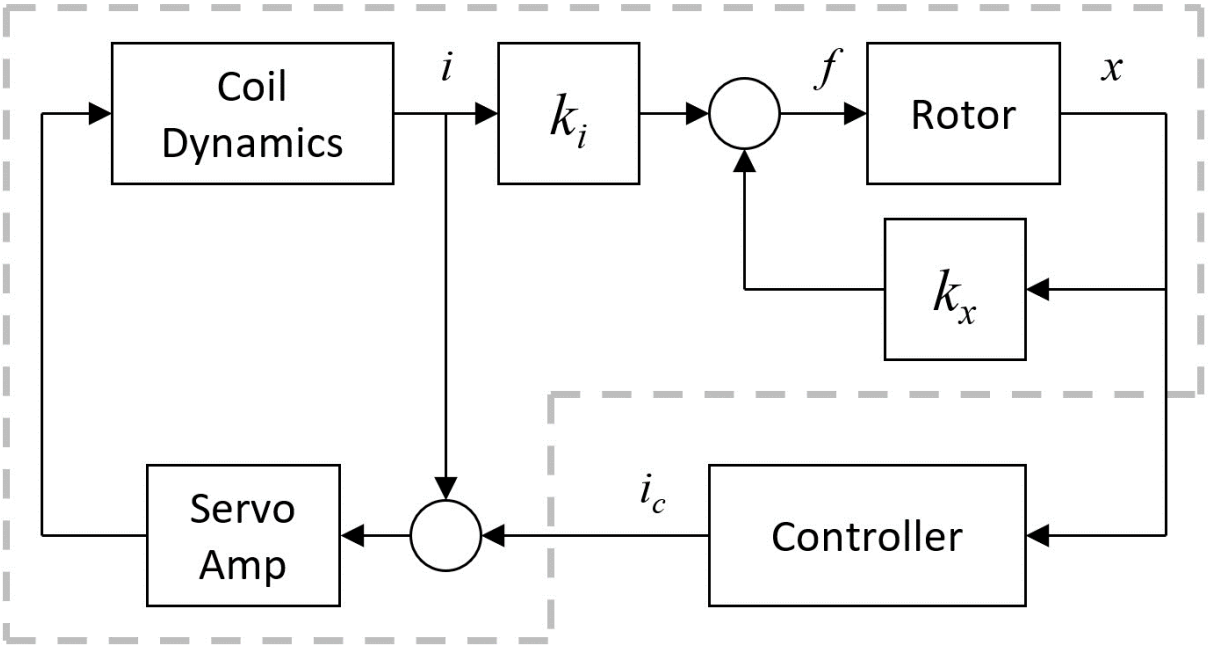


a)

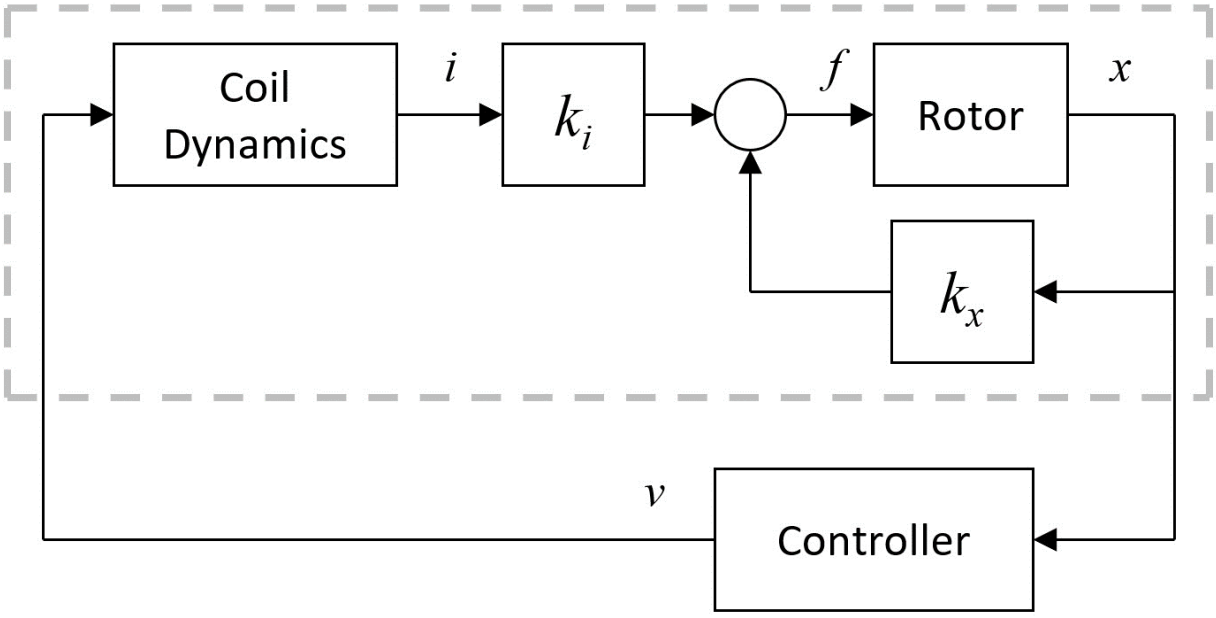


b)

*Fig 1.2. AMB control schemes, a) typical current control, and b) simple voltage control.*

The second scheme is a voltage control that utilizes digital controls. The architecture has a digital signal processor, analog-to-digital converter and a digital-to-analogue converter [[4]. Usually, these components come in a single microprocessor board which has additional memory, filters, and peripherals to connect to other devices. In this configuration, the digital controller generates a PWM signal from the sensor error signal input. The PWM signal controls amplifiers or transistor switches which control the overall current supplied to the electromagnets, hence controlling the magnitude of the magnetic field generated as shown in Fig 1.2) b.

The current work focuses on voltage digital control which is superior to the conventional current control in some ways. The digital control scheme offers high flexibility which has a number of advantages including: tuning control parameters easily, viability of implementing complex control algorithms, unbalanced control, flexible set point for different process states, possibility of monitoring operating conditions of the AMB such as position, current and vibration, and most importantly feasibility of incorporating the system on the internet which enables remote diagnosis, predictive maintenance, advanced communication and remote control. Even though both voltage and current control schemes can offer these advantages, voltage control is implemented with fewer parts and less circuitry making it less costly and compact as compared to the current controlled scheme.

## 1.1 Characteristics and Advantages of Active Magnetic Bearings

Active magnetic bearings have no physical contact between the stator and the rotor. The contactless nature of the bearing means no lubrication and no frictional wear is experienced [[5]. Making these bearings ideal in vacuum applications, food industry and sterile rooms where high hygiene and contamination free environments are required. The airgap between the stator and the rotor can range from a faction of a millimeter to about 20 millimeters (about 0.79 in) depending on the application [[1]. In high precision applications the airgap is small to enable precise and robust control.

Active magnetic bearing rotors can achieve very high speeds. Ideally, the speed that can be achieved is limited by the material strength of the rotor. With traditional rolling element

bearings, the rolling elements have larger radius of rotation than shaft limiting the maximum size of shaft that is supported. The possibility of high speeds makes the design and construction of the AMBs flexible. Greater shaft diameters and high-power density can be achieved making the shaft less susceptible to vibrations due to increased stiffness. Industrial magnetic bearings can run at 5 to 20 times the operating speeds of ball bearings [[2].

The closed-loop dynamics of an AMB can be modelled as a spring mass damper system with stiffness and damping coefficients. Since the AMB control is accomplished by a microprocessor, these parameters can be adjusted within the physical limits of the bearing's application and operating condition. It is therefore possible to use the bearing as vibration isolators, operating at or beyond the critical speeds within the recommended vibrations and stabilizing the rotor if excited by an external disturbance.

Active rotor position control makes it possible for the AMBs to be applied in precision industries. Precision measurement is dependent on the resolution of the sensors used and the fidelity of the control signal. Using high resolution sensors and adopting a noise resistance circuit makes It possible to precisely control the position of the rotor.

Since there is no contact between the rotor and the stator, there is minimal frictional wear on the bearing, making it last longer and ideal to be used in applications that require minimal maintenance [[1]. The AMBs also do not need lubrication, therefore there is an overall reduction in the maintenance and operation cost. With minimal power losses and possibility of achieving high speeds, AMBs can achieve higher efficiencies and last longer than conventional bearings.

The possibility of integrating the active magnetic bearings into the internet via the control electronics opens a whole range of opportunities where health monitoring, remote control and dynamic system testing is possible. These eliminate the need for physically checking the condition of the AMB or performing corrective maintenance. Usually, to change the dynamics properties of a conventional bearing, the bearings must undergo the entire process of redesigning, prototyping, testing, manufacturing and installation. This is not the case when it comes to active magnetic bearings, the dynamic properties of active magnetic bearings which include the stiffness, and damping can be adjusted within the bearing controller [[6].

## 1.2 History of AMBs

The history of active magnetic bearings dates to a theory from the 19$^{th}$ century. In 1842, Earnshaw's Theorem stated that point charges cannot be maintained at a stable equilibrium by an electromagnetic force from the charges independently [[7]. The theorem also extends to electrostatic, magnetostatic and gravitational force. Meaning it is impossible to have stable levitation by means of passive magnetic fields. Therefore, to overcome this limitation, a time varying field, a superconductor for diamagnetism or an actively controlled feedback system can be used. Active feedback control is the most used practical approach to overcome Earnshaw's Theorem.

In 1937, a patent by Kemper demonstrated the potential of active magnetic bearings for application in the vehicle transport industry [[1]. Also in Beam's experiment, he managed to demonstrate active magnetic levitation by rotating a tiny shaft at recording breaking speeds of 800

thousand revolutions per second while the rotor is supported by magnetic fields. It was not until 1974 that the real application of AMBs in rotor dynamics was displayed [[8]. More research interests especially in the aerospace industry led to the development of a rate gyro for directly getting the angular rates from a control signal of an AMB. Similarly, AMBs were used for altitude satellite control which was achieved by levitating a momentum wheel. With the development of solid-state electronics, digital controls and reduced size of microcontrollers, AMBs have gained a wide range of applicability over time.

For the past two decades, advancements in modelling systems, advanced design tools, and new control strategies have driven the research of AMBs further. In high-speed industrial applications research has shown that motors and generators with AMBs can achieve tangential speeds up to 340 m/s if a rotor with enhanced mechanical and magnetic properties are used [[9]. Research has also focused on control of elastic rotors. Controlling of elastic rotors is more complex as opposed to rigid rotors supported by an AMB. Flexible rotors in high speeds experience unbalancing at individual critical speeds at different number of planes along the length of the rotor, hence the need for a unified balancing method or modal balancing [[10].

In case of a loss of levitation at high speeds the contact between the stator and the rotor can lead to very high vibrations and damage. To mitigate this condition, AMB rotors have extra conventional bearings which come into action in case such an extreme situation occurs. The dynamics of these touch down bearings have not been fully understood due to their nonlinearity, uncertainties with phases and strong reliance of initial conditions [[11]. Therefore, designing the

combination of AMB with touch down bearings requires experience since a systematic design procedure has not been developed yet.

Further and most recent research is based on smart machinery which incorporates the sensing, actuating and data processing capabilities of machinery to perform self-correction, tuning, calibrations and diagnostics. A theoretical model has been developed to show how AMBs can be implemented as smart machines [12]. The model divides the smart AMB into three levels, the first level is the mechatronics level that comprises of the sensing, controlling and actuating hardware. The second level is a software model of the physical hardware that represents the actual AMB components as mathematical models. This model guides the controller parameter design of the real AMB. The third level is the information systems management level that can collect relevant data from the AMB and provide the data in a GUI which can be interpreted an operator. Fig 1.3 illustrates the three-level model of a smart AMB.

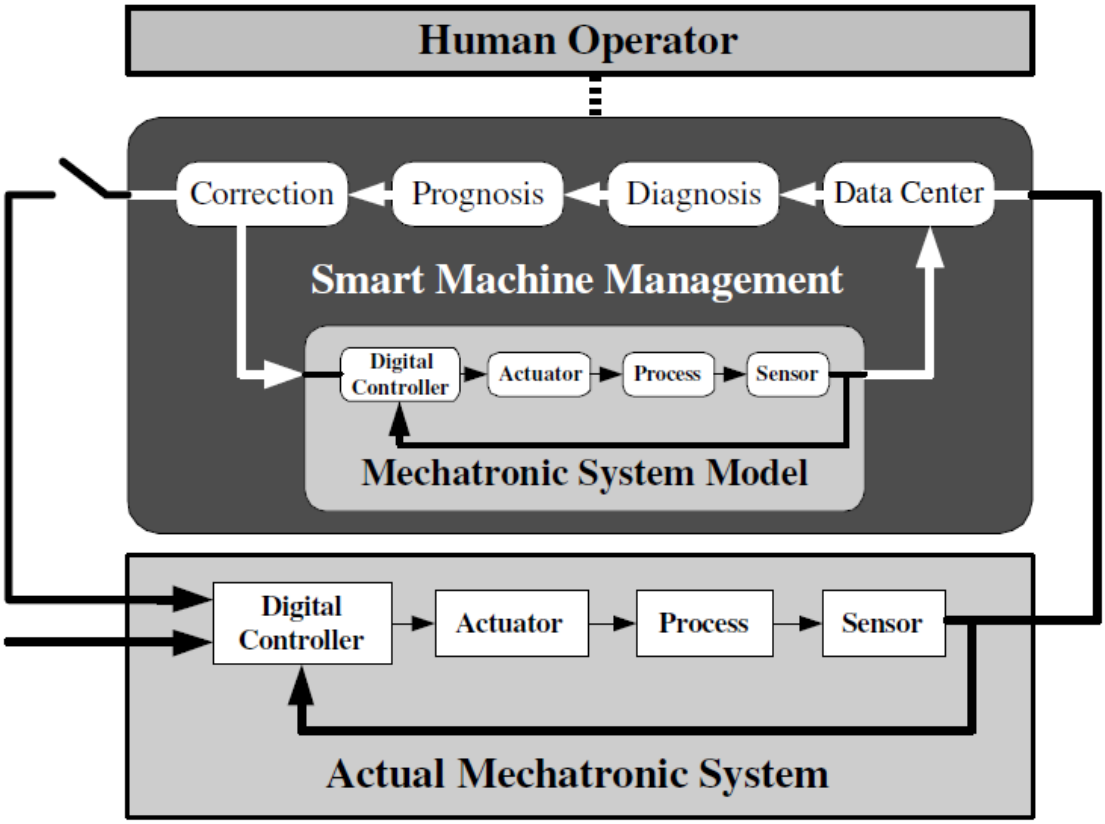


*Fig 1.3. A concept model of a smart AMB* [12].

## 1.3 History of IoT

Despite Active magnetic bearing being in existence since the 1980s, the concept of Internet-of-Things was conceived around 2008 and 2009 [13]. This was well after the invention of the internet and maturity of the internet technology in facilitating communication across the globe. The term referred to a huge number of electronic devices being connected to the internet. The development of IPv6 internet protocol in 2011 opened new opportunities in the IoT industry since the protocol offered unlimited possibility of addressing ideally every atom on Earth [14].

Prior to the development of IoT, the industry was adopting technologies in automation such as programmable logic controllers which date back to 1968 when they were invented [[15]. With the emergence of electronic smart devices such as phones and laptops, the concept of IoT was deemed viable in the industrial set up. This was due to these devices having input/output components, processors, data storage, and networking elements. Since the industry needed a better way of collecting data, processing and communicating with different machine elements within a manufacturing set up the Industrial Internet of Things came into existence.

IIoT technology was aimed at connecting industrial sensors with their respective software. Furthermore, the IIoT provided a human interfacing platform with connected machines. IIoT improved existing automation technologies such as PLCs and SCADA [[13]. Now data collected from sensors is not only monitored but it can be processed and analyzed to give meaningful feedback to control a process. With advancements in technology, self-diagnosis, self-correction, and self-control became a potential reality.

## 1.4 Features of IoT

Some of the key feature of IoT include:

**Connectivity [**[13]**:** For IoT to exist, there is need for a linking networking irrespective of the location of the devices. For these devices or machines to be connected, the network must be accessible and compatible with each device.

**Dynamic changes and adaptations [**[15]**:** the IoT technology keeps changing, the connected devices or machine elements should be able to adapt to the constantly changing

dynamics. An example is with the increasing number of devices over time, IoT gateways should be able to accommodate increased sensor node points. Sensors also should gather data in any condition, with the ability to self-adjust to the prevailing conditions.

**Scalability [**[13]**:** Its important the IoT technology be scalable due to the exponential increasing of connected devices over a short period of time. Data collection, management, processing and interpretation should be efficient regardless of the number of devices connected.

**Interoperability of communication protocols [**[14]**:** IoT devices should support seamless communication with each other. If one device is using a different communication protocol from another, they should be able to communicate with each other.

**Embedded Intelligence [**[6], [16]**:** IoT devices should have the ability to process and provide useful information from the data provided by the sensors. Some sensors have built in microprocessors that perform data preprocessing before linking the data to a cloud platform or a gateway.

**Safety:** Safety is a key consideration since IoT involves data transmission over the internet which is not always safe. Therefore, as we leverage on the benefits of IoT, we should have in mind the protection of the data and personal information being sent online. Security should not only be on the network but also at the node points where physical elements such as sensors are collecting data and the receiving endpoint where IoT data is used to perform an action such as controlling some machine element.

**Embedded sensors and actuators [**[16]**:** sensors provide the link to the physical environment by identifying and quantifying different environmental parameters. Incorporating them in every device that has processing and networking capability enables a better representation of our surroundings. Actuators perform the real task of providing desired mechanical, electrical, magnetic, hydraulic or pneumatic motion.

**Data:** Finally, IoT does not exist without data. The reason for connecting all these devices to the internet is basically to be able to collect, process, transmit and interpret data to improve a process, make better decisions or control another process.

## 1.5 Applications and Benefits of IoT

Industrial IoT has gained traction especially in the manufacturing sector where the supply chain monitoring is crucial. Companies have leveraged IoT to manage their fleet, track products on the assembly line and monitor processes remotely [[15]. IoT opened a door for predictive maintenance by incorporating sensors in machines and monitoring the sensor data overtime. Failure of the machine element can be predicted before the actual failure occurs. The benefits of IoT in the industry overall can be summarized by the following:

**Digital connection and remote management** [17]**:** by connecting equipment or machinery with users, partners, engineers and manufacturers, information about the performance of the equipment is easily shared and stakeholders can make quick decisions on key issues involving the equipment of the machine. Managers can remotely monitor and supervise the

operation of machines without physically walking around the factory to make sure everything works well.

**Facility management** [15]**:** With machines equipped with sensors that can collect data and send it to a remote user which enables condition-based maintenance and repair, the facility management can use this data to make decisions on when to schedule maintenance, and times to run the machines on full load or lesser loads. Plan on what kind of parts to order for maintenance in time to reduce lead times. Eventually, the facility will reduce energy waste, cost of maintenance and operation of the facility and improve efficiency.

**Auto supervision [**[14]**:** Real time monitoring of a product through its entire life cycle using IoT helps in eliminating industrial waste that can be incurred along the way. Intelligent machines embedded with sensing and actuation capabilities can perform supervisory on the industrial line while a remote user just oversees the process [[14].

**Safety and security** [13]**:** IoT have provided real time communication of industrial machines with handheld devices where activities of the machine can be monitored, potential failure, wear, or malfunction of a machine can be identified which significantly reduces the injuries that would been incurred if the machine was being operated by a human.

**Reduced downtime** [[15]**:** Armed with IoT data collected overtime, proper planning of equipment maintenance, inventory restocking, and industrial waste management strategies can be implemented at the right time reducing unnecessary machine downtime.

**Better data analysis** [[14]**:** IoT data from machines and equipment can be collected and exported to other software for further analysis. Advanced data analysis that is not offered by most IoT devices can give more insight into the state of the equipment or machine.

Some benefits of IIoT to manufacturing are summarized in Fig 1.4.

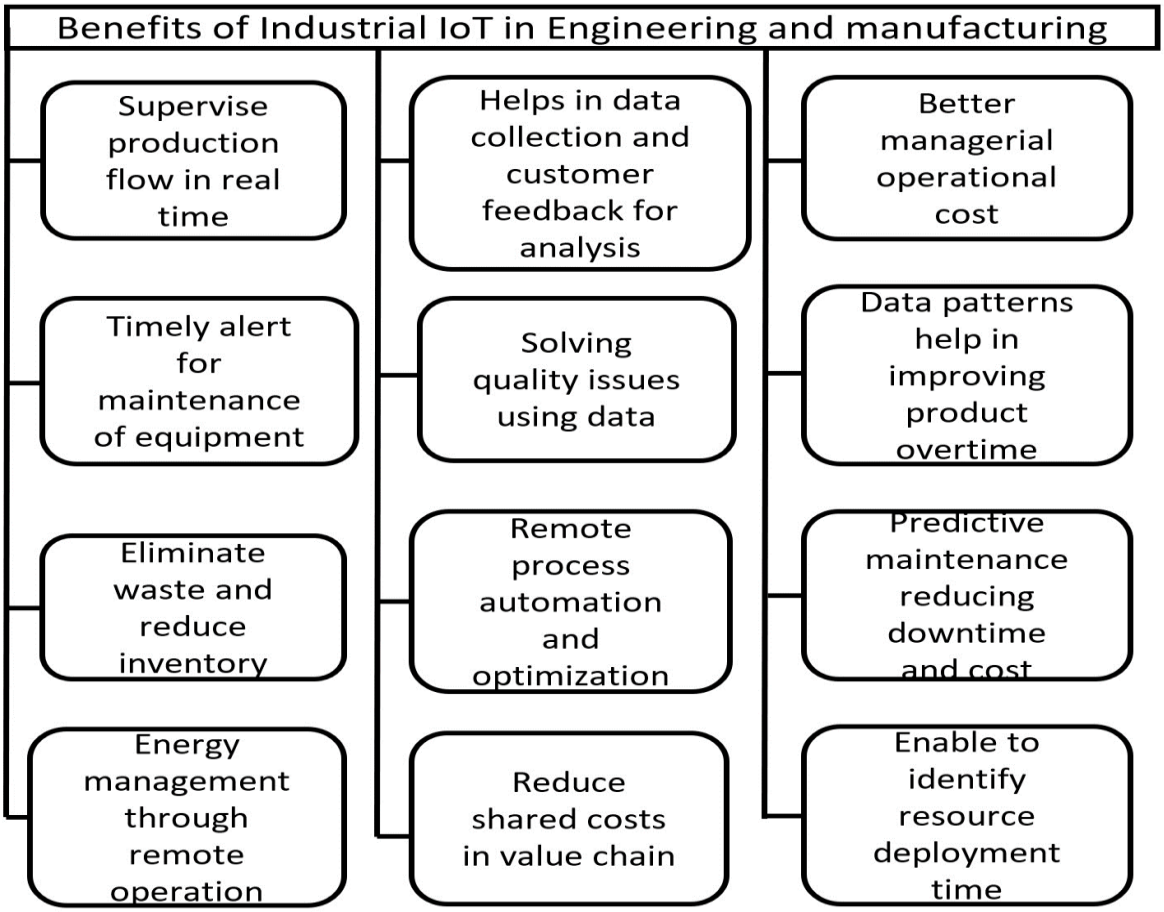


*Fig 1.4. Benefits of IoT in engineering and manufacturing.*

Apart from industrial equipment and machine integration to IoT, there are many other industries that IoT has benefited from significantly. Home automation where appliances are

remotely controlled via the internet. Smart agriculture where the temperature, humidity and greenhouse lighting, and soil moisture content are actively monitored. In the medical field, where the patient's health condition can be monitored. The temperature, heart rate, blood pressure of a patient can be remotely monitored while the patient is at home. Other industries include education, smart cities, traffic monitoring, energy management, vehicle connection, and any other sector that data can be collected and utilized to improve, control or develop a process.

## 1.6 Scope of work

This work presents the design and development of a voltage controlled active magnetic bearing. The voltage controlled AMB has two electromagnets which control a rotor in a single axis. A controller performs the control action with the aid of transistors which act as switches.

The AMB is integrated to the internet via an IoT gateway. Data from sensors on the AMB collect data and sends it on the cloud. The data can be accessed via an IoT cloud Platform for analysis and visualization. In this case, the ThingSpeak IoT platform was used to access the AMB sensor data. The data was monitored in real time and visualized on the graphic user interface.

A program was developed to send command signal remotely to the AMB. One of the command signals used for the purpose of this research was a step response performed remotely and monitoring how the system responds. The remote step response was compared with a similar step response that was performed locally.

Finally, MOSFET and GaN transistors switching action was compared on the voltage controlled AMB. Their performance was evaluated the switching time and power consumption

during the switching action. The comparison was important to evaluate the type of transistor that will offer better performance of the AMB and can be applicable in the industry.

## 1.7 Organization of the thesis

The thesis consists of five chapters. The first chapter introduced the AMB technology by giving a brief history of the invention of the technology. It outlines how the technology developed into the current industrial AMBs. The characteristics and general application of AMB is also discussed. IoT history and features are also introduced here. Finally, the chapter discusses how IoT applications inclined towards the industry and machinery for remote monitoring and control.

In the second chapter, the AMB principles and IoT architecture is discussed in detail. The AMB governing equations for a single axis levitation SISO system are derived. The mathematical modelled equations were transformed from time domain into the frequency domain for analysis in SIMULINK. The chapter further discusses the control law utilized in AMBs. A detailed interaction between the AMB hardware and software in implementing the sensing and actuation is also outlined. The chapter concludes with a comprehensive IoT architecture detailing the integration of machinery into the Internet and communication protocols used to achieve the integration.

Chapter Three of this work talks about experimental test rig development. The steps towards the development of the test rig and integrating it onto the Internet are outlined. The electromagnetic circuit, sensor circuit and the IoT circuits were detailed. The chapter dives into how key parameters of the AMB test rig, which include the force displacement factor and the force current factor are obtained experimentally and analytically. PID tuning, performing a local and remote step response

to evaluate system performance is also included in this chapter. Finally, the comparison of GaN and MOSFET applied in the integrated AMB test rig is outlined.

Chapter Four discusses the results obtained from the experimental determination of the force displacement factor and force current factor parameters and compared to the analytical values. The results from the step response performed locally and remotely are also compared. The remote step response performance was evaluated by calculating the latency of the response compared to the signal latency of the local response. The remotely monitored results via ThingSpeak IoT cloud platform were also displayed in this chapter. The results of the comparison of the GaN and MOSFET transistors' performance as applied to the integrated AMB are discussed.

Chapter Five concludes this work by discussing the results and their impact on the current and future research in AMB integration to the internet of things and smart machinery in general. The contributions of this research are outlined together with potential research avenues identified.

# 2 AMB PRINCIPLES, IOT ARCHITECTURE, AND LITERATURE REVIEW

Active magnetic bearings utilize the principle of electromagnetic induction to generate magnetic field that attracts a ferromagnetic target. The electromagnetic principle is when electric charges flow through a coil inducing a magnetic field that is perpendicular to the flow of the electric current. The main components of an active magnetic bearing include sensors, actuators, controller, and rotor [18]. Electromagnets are actuators since they generate the magnetic field that supports the rotor. The sensors are used to locate the position of the rotor and report in real time to the controller. The controller performs the control action by generating a control signal which is invoked to control the amount of current the electromagnets are receiving.

The weight of the rotor to be levitated dictates the amount of static force that will be generated by the electromagnets. The force is directly proportional to the square of the current that is supplied to the electromagnets and inversely proportional to the square of the airgap [19]. Therefore, to control the levitation, the force generated is controlled by controlling the current supplied to the electromagnets in reference to the position of the rotor. The sensing and actuation ability of AMBs make it viable to be integrated into the internet of things since IoT involve the connection of devices with the sensing, actuating, data transfer, and data processing capabilities on the internet so that they can exchange information and perform required actions.

## 2.1 Working Principles of AMBs

In a single axis active magnetic bearing system, there are two coils that position in one axis on opposite sides of the rotor which lies between the two coils. The coils are basic RL circuits with power supply, while the rotor is a free mass as shown in Fig 2.1.

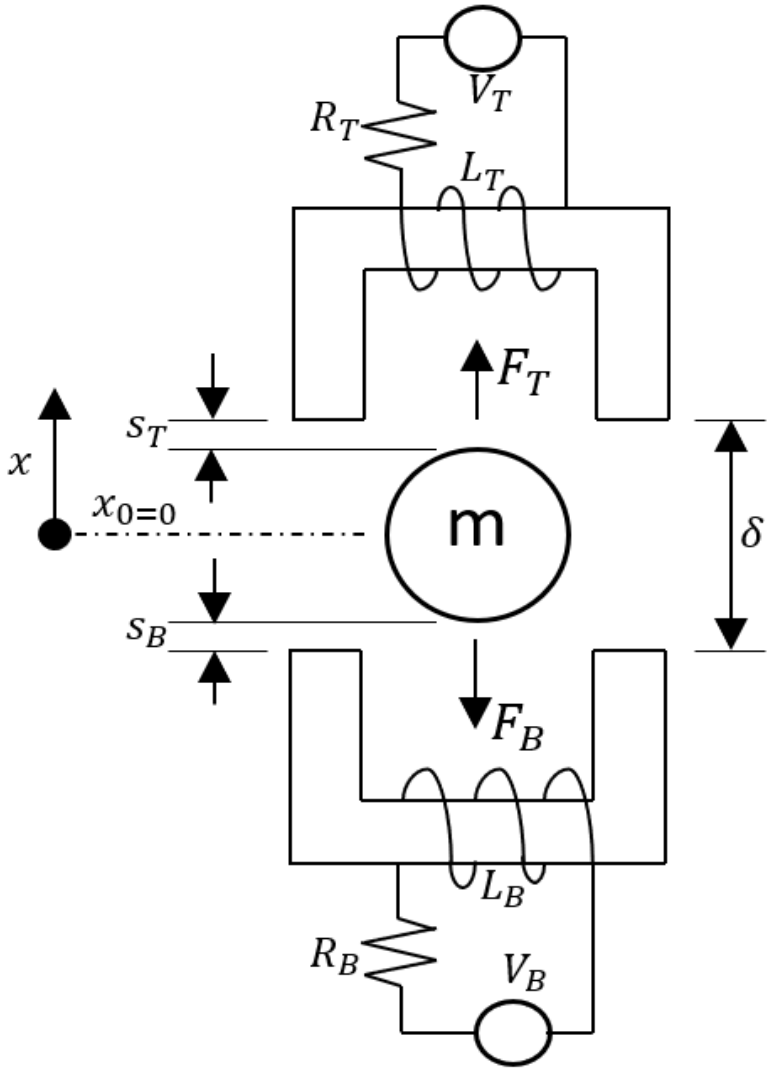


*Fig 2.1. Single axis active magnetic bearing schematic.*

Initial position, $x_0$, represents the equilibrium position of the rotor represented by mass, $m$. The airgaps $s_T$ & $s_B$ represents the airgap between the top and bottom electromagnet, respectively. $R_T$ & $R_B$ are the resistances in the electromagnetic circuits, $L_T$ & $L_B$ are the inductances of each circuit. The force generated by the electromagnets is represented by $F_T$ & $F_B$. From Newtown's Second Law of motion the system forces can be summarized as:

$$\boldsymbol{m\ddot{x} = \sum F} \tag{2.1}$$

$$\boldsymbol{m\ddot{x} = F_T - F_B + F_D} \tag{2.2}$$

Where $F_D$ represents the external force disturbances on the rotor.

### 2.1.1 Bearing Electromagnetism

The mechanical force acting on the rotor is because of the electrical induction which is represented by Lorentz force which acts perpendicular to the velocity of electric charge, $Q$ [1]. The velocity of the charge is perpendicular to the magnetic field vector $\bar{B}$. The force is calculated by a cross product between the velocity of the electric charge and the magnetic field vector perpendicular to the velocity.

$$\boldsymbol{f = Q(\bar{v} \times \bar{B})} \tag{2.3}$$

The magnetic flux in a straight conductor is represented by circular lines around the conductor with an arrow showing the direction of the vector fields. The flux density of the

magnetic fields is usually visualized by the density of the lines in an area. The total flux, Φ within a certain surface area, $A$ can be found by performing a surface integral of the flux density over that area.

$$\boldsymbol{\Phi} = \iint_{\mathbf{A}} \overline{\mathbf{B}}.\, \mathbf{d}\overline{\mathbf{A}} \tag{2.4}$$

When the flux density is constant in the entire area, then the total flux becomes:

$$\boldsymbol{\Phi} = \mathbf{BA} \tag{2.5}$$

### 2.1.2 Magnetic Circuit

The magnetic circuit analogized with the electric circuit. Table 2.1 shows the analogy between an electric circuit and a magnetic circuit.

*Table 2.1. Analogy between electric and magnetic circuits* [20]

| Electrical | Magnetic | Magnetic units |
|---|---|---|
| Voltage $v$ | Magnetomotive force $\mathcal{F} = Ni$ | Amp-turns |
| Current $i$ | Magnetic flux $\phi$ | Weber Wb |
| Resistance$R$ | Reluctance $\mathcal{R}$ | Amp-turns/Wb |
| Conductivity $\frac{1}{\rho}$ | Permeability $\mu$ | T-m/A |
| Current density $J$ | Magnetic flux density $B$ | $Wb/m^2 = T$ |
| Electric field$E$ | Magnetic field intensity $H$ | Amp-turn/m |

In a simple magnetic circuit with an airgap, the circuit is almost like the voltage, resistance circuit of an electric circuit but in this case the resistance is the core and the airgap magnetic field resistance while the voltage will be the magnetomotive force.

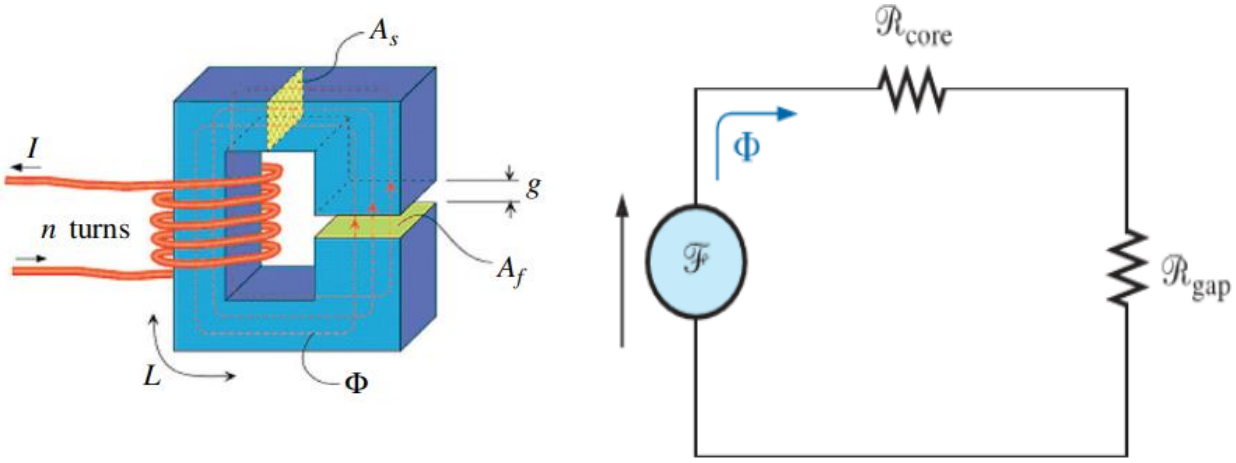


a. Magnetic circuit with airgap.

b. Magnetic circuit diagram.

*Fig 2.2. A simplified magnetic circuit diagram* [21].

Where, $g$ is the airgap, $L$ is the coil inductance, $A_s$ is the core cross section area, $A_f$ is the cross-section area of the of the airgap, $\Phi$ is the total flux, $n$ is the number of coils, $I$ is the current, $\mathcal{R}_{core}$ is the resistance of the core, and $\mathcal{R}_{gap}$ is the resistance of the airgap.

Applying Ampere's law to the magnetic circuit in Fig 2.2.

$$\mathbf{NI} = \boldsymbol{\Phi}\left(\boldsymbol{\mathcal{R}}_{\mathbf{gap}} + \boldsymbol{\mathcal{R}}_{\mathbf{core}}\right) \tag{2.6}$$

$$\mathbf{NI} = \boldsymbol{\Phi}\left(\frac{\mathbf{g}}{\boldsymbol{\mu}_0\mathbf{A_f}} + \frac{\mathbf{l_c}}{\boldsymbol{\mu}_0\boldsymbol{\mu}_c\mathbf{A_s}}\right) \tag{2.7}$$

Where, $\mu_0$ is magnetic permeability of a vacuum, and $\mu_c$ is relative permeability of the core. For the case of a single axis magnetic bearing shown in Fig 2.1, there are two airgaps in a single magnetic circuit and the cross-section area is the same throughout the magnetic core and the airgap.

$$\mathbf{A = A_f = A_s} \tag{2.8}$$

$$\mathbf{NI = BA\left(\frac{2g}{\mu_0 A} + \frac{l_c}{\mu_0 \mu_c A}\right)} \tag{2.9}$$

$$\mathbf{\mu_0 NI = B\left(2g + \frac{l_c}{\mu_c}\right)} \tag{2.10}$$

$$\mathbf{B = \frac{\mu_0 NI}{\left(2g + \frac{l_c}{\mu_c}\right)}} \tag{2.11}$$

Since the $\mu_c \gg 1$ *in iron the magnetization is neglected*

$$\mathbf{B = \mu_0 \frac{NI}{2g}} \tag{2.12}$$

The inductance $L$ of the magnetic circuit is the ratio of the winding flux $\Phi_w$ from a single turn in the coil to the current $i$. For a coil with $N$ turns the total inductance is.

$$\mathbf{L} = \frac{\mathbf{N\Phi}}{\mathbf{i}} \tag{2.13}$$

Knowing $\Phi = BA$

$$\mathbf{L} = \frac{\mathbf{NBA}}{\mathbf{I}} = \frac{\mathbf{\mu_0 N^2 A}}{\mathbf{2g}} \tag{2.14}$$

### 2.1.3 Electromagnetic Force

The electromagnetic forces generated at the boundary between the differing permeability is calculated based on the energy stored in the airgap volume. If the airgap volume $V_f = 2gA_f$, then the energy stored in this volume is expressed as:

$$\mathbf{W_f} = \frac{\mathbf{1}}{\mathbf{2}}\mathbf{B_f H_f V_f} = \frac{\mathbf{1}}{\mathbf{2}}\mathbf{B_f H_f A_f (2g)} \tag{2.15}$$

The energy is expressed mechanically as an attractive force which is found by the partial derivative of the energy equation with respect to the airgap.

$$\mathbf{F} = -\frac{\mathbf{\partial W_f}}{\mathbf{\partial g}} = \mathbf{B_f H_f A_f} \tag{2.16}$$

Since $H_f = \frac{B_f}{\mu_0}$, $B_f = \mu_0 \frac{NI}{2g}$

$$\mathbf{F = \frac{B_f^2 A_f}{\mu_0} = \mu_0 A_f \left(\frac{NI}{2g}\right)^2 = \frac{1}{4}\mu_0 N^2 A_f \frac{I^2}{g^2} = k\frac{I^2}{g^2}} \quad 2.17$$

$$\mathbf{k = \frac{1}{4}\mu_0 N^2 A_f} \quad 2.18$$

Applying the force equation to the single axis magnetic bearing force equation becomes

$$\mathbf{F_T = k\left(\frac{I_T}{s_T}\right)^2, F_B = k\left(\frac{I_B}{s_B}\right)^2} \quad 2.19$$

$$\mathbf{m\ddot{x} = F_T - F_B + F_D = k\left(\frac{I_T}{s_T}\right)^2 - k\left(\frac{I_B}{s_B}\right)^2 + F_D} \quad 2.20$$

$$\mathbf{\ddot{x} = \frac{k}{m}\left(\frac{I_T}{s_T}\right)^2 - \frac{k}{m}\left(\frac{I_B}{s_B}\right)^2 + \frac{1}{m}F_D} \quad 2.21$$

### 2.1.4 Electrical circuit analysis

According to Faraday's Law the back EMF induced in the coil can be expressed as:

$$\mathbf{v_E = N\frac{d\phi}{dt}} \tag{2.22}$$

From Kirchoff's Voltage law, the coil circuit can be expressed as:

$$\mathbf{V = IR + L\frac{dI}{dt} + N\frac{d\phi}{dt}} \tag{2.23}$$

$IR$, is the voltage drop as a result of coil resistance and $L\frac{dI}{dt}$, is the voltage drop due to coil self-inductance.

$$\mathbf{\frac{d\phi}{dt} = \frac{2k}{N}\frac{d}{dt}\left(\frac{I}{g}\right)} \tag{2.24}$$

$$\mathbf{V = IR + L\frac{dI}{dt} + 2k\frac{d}{dt}\left(\frac{I}{g}\right)} \tag{2.25}$$

Therefore, the top and bottom coil voltage becomes:

$$\mathbf{V_T = I_T R_T + L_T\frac{dI_T}{dt} + 2k\frac{d}{dt}\left(\frac{I_T}{s_T}\right)} \tag{2.26}$$

$$\mathbf{V_B = I_B R_B + L_B\frac{dI_B}{dt} + 2k\frac{d}{dt}\left(\frac{I_B}{s_B}\right)} \tag{2.27}$$

### 2.1.5 Force-Current ($k_i$) and Force-Displacement ($k_x$) Relation

Due to the nonlinear nature of the equation of motion of the active magnetic bearing, for purposes of designing control systems for AMB, a linear relation is preferred [22]. The equation can be approximated to be a linear function around the operating point. Industrial active magnetic bearings usually operate at a differential drive mode where the force generated by the top electromagnet is because of the total control current, $i_x$ and the bias current, $i_0$ while the bottom magnet is supplied with the bias current less the control current. The force experience by the rotor, $F_x$, at an instantaneous position assuming no external disturbances can be expressed as:

$$\mathbf{F_x = F_T - F_B} \tag{2.28}$$

When the rotor is exactly at the mid position between the two coils, the airgaps are equal.

$$\mathbf{s_T = s_0}, \qquad \mathbf{s_B = s_0} \tag{2.29 a, b}$$

If the rotor moves a distance $x$ towards the top coil, the airgap changes to:

$$\mathbf{s_T = s_0 - x}, \qquad \mathbf{s_B = s_0 + x} \tag{2.30}$$

Therefore, the force experienced by the rotor at this instantaneous position is expressed as:

$$\mathbf{F_x = k\frac{(i_0 + i_x)^2}{(s_0 - x)^2} - k\frac{(i_0 - i_x)^2}{(s_0 + x)^2}} \tag{2.31}$$

By linearizing around the operating point $(i_0, s_0)$.

$$\mathbf{F_x = \frac{\partial F_x}{\partial i_x}(i_0, s_0)i_x + \frac{\partial F_x}{\partial x}(i_0, s_0)x} \tag{2.32}$$

$$\frac{\partial \mathbf{F_x}}{\partial \mathbf{i_x}} = \frac{\mathbf{2k(i_0 + i_x)}}{\mathbf{(s_0 - x)^2}} + \frac{\mathbf{2k(i_0 - i_x)}}{\mathbf{(s_0 + x)^2}} \quad 2.33$$

$$\left.\frac{\partial \mathbf{F_x}}{\partial \mathbf{i_x}}\right|_{\mathbf{i_x=0,\ x=0}} = \frac{\mathbf{4ki_0}}{\mathbf{s_0^2}} \quad 2.34$$

$$\frac{\partial \mathbf{F_x}}{\partial \mathbf{x}} = \frac{\mathbf{2k(i_0 + i_x)^2}}{\mathbf{(s_0 - x)^3}} + \frac{\mathbf{2k(i_0 - i_x)^2}}{\mathbf{(s_0 + x)^3}} \quad 2.35$$

$$\left.\frac{\partial \mathbf{F_x}}{\partial \mathbf{x}}\right|_{\mathbf{i_x=0,\ x=0}} = \frac{\mathbf{4ki_0^2}}{\mathbf{s_0^3}} \quad 2.36$$

$$\mathbf{F_x} = \frac{\mathbf{4ki_0}}{\mathbf{s_0^2}}\mathbf{i_x} + \frac{\mathbf{4ki_0^2}}{\mathbf{s_0^3}}\mathbf{x} \quad 2.37$$

In which

$$\mathbf{k_i} = \frac{\mathbf{4ki_0}}{\mathbf{s_0^2}}, \quad \mathbf{k_x} = \frac{\mathbf{4ki_0^2}}{\mathbf{s_0^3}} \quad 2.38$$

$$\mathbf{F_x = k_i i_x + k_x x} \quad 2.39$$

## 2.2 AMB Control Laws

There are different techniques used to control AMBs. This section discussed the most used control techniques, the state-of-the-art techniques, and what is implemented for the purpose of this research.

### 2.2.1 PID Control of AMB

PID controllers are the most common and basic type of controller that is applied in industrial AMBs. The working principle of the PID controller involves the position sensor measuring the rotor instantaneous position, the position is compared with a desired position and the difference is an error signal (e). The error signal is applied to different gains namely, proportional gain $(k_p)$, the derivative gain $(k_d)$ and the integral gain $(k_I)$ to generate a control signal. The proportional gain acts like a mechanical spring gain, the derivative gain is more of like a damper and the integral gain reduces the steady-state error [23].

In the case of an AMB, the proportional gain helps the system to respond faster, the derivative gain prevents the system from too much overshooting and the integral helps in reducing errors at steady state. The overall effect of the controller is the sum of the three contributions which help in gaining stability. Equation 2.40 presents the control effort signal in time domain and the control law transfer function with the respective gains is presented in equation 2.4, where $\boldsymbol{\tau_d}$ is the filter gain.

$$\mathbf{C_{PID}(t) = K_p e(t) + K_d \frac{de(t)}{dt} + K_i \int e(t)dt} \quad 2.40$$

$$\mathbf{C_{PID}(s) = K_p + \frac{K_d s}{\tau_d s + 1} + \frac{K_i}{s}} \quad 2.41$$

### 2.2.2 LQR and LQG Control

Linear quadratic regulator (LQR) control is simple optimal control and when used with a Kalman filter for estimating the state vector linear quadratic gaussian (LQG). Given a LTI system, the LQR controller is designed to minimize the quadratic cost function $J$ on state vector $x$, and control effort vector $u$ to obtain an optimal gain $K$ [23].

$$\mathbf{J = \int_0^\infty (x^T Q x + u^T R u) dt, \;\; u = -Kx} \quad 2.37$$

Where $Q$ is weight on the states, $R$ weight on input, $x$ is the weighted state, and $u$ is the input signal.

### 2.2.3 $H_\infty$ Control

This method is common in modern AMB control. The objective of the $H_\infty$ control is to minimize response in the presence of uncertainties and disturbances on the systems often expressed as the difference between frequency response of the actual system and the ideal system. The robustness of the system is achieved when the uncertainty loop gain is less than one from the Linear fractional transformation (LFT) model in Fig below [23].

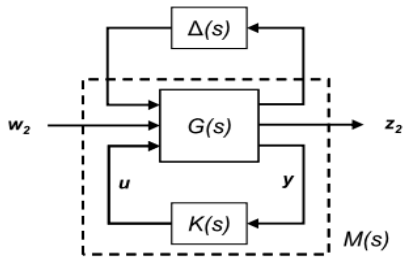


*Fig 2.3. LTF of a closed loop system* [23].

$$|\mathbf{M(j\omega)\Delta(j\omega)}| < \mathbf{1} \tag{2.38}$$

### 2.2.4 $\boldsymbol{\mu}$ Synthesis

This method aims at designing a controller with a $\mu - value$ below a certain set value for the system to have robust stability and performance [24]. The $\mu - value$ is defined as:

$$\boldsymbol{\mu_{\Delta}(M)} = \frac{\mathbf{1}}{\mathbf{\min\{\bar{\sigma}(\Delta):\det(I - M\Delta) = 0, \Delta \text{ is structured}\}}} \tag{2.39}$$

It differs from the $H_\infty$ in that the uncertainty of the system is parametric making it possible to deal with coefficient uncertainty at component level.

### 2.2.5 Self-tuning, Neural Network and Adaptive Control

With advancement in artificial intelligence self-tuning controls based on LQG objective functions have been employed. Neural network models such as Confidence Interval Network (CIN) and Radial Basis Function Network (RBFN) have been employed to observe system uncertainty for $H_\infty$ control [25].

### 2.2.6 Digital Signal Processing Control

A modern trend in controlling AMB, which is the state-of-the-art in motor control, involves the use of a digital signal processor with peripherals that direct the PWM signal to control the AMB. This current trend especially works well with voltage controlled active magnetic bearings like the one used in this research. It eliminates the need to create a system control software and another hardware part for the underlying current control loop in a typical current controlled AMB. In the digital signal processing only the system control software e.g., PID control algorithm is required to process the error in a microcontroller and generate the appropriate control signal in form of a PWM signal. It is possible to implement more complex control topologies using this voltage controlled digital signal processing technique. This research leveraged this technique to control the AMB.

## 2.3 IoT Architecture for AMBs

AMBs have sensors and actuators that can be linked through relevant communication channels and protocols to offer a fully integrated IoT system. The architecture has five layers which include the perception layer, network layer, data processing layer, and the application layer as shown in Fig 2.4. For an AMB, these layers correspond to IR position sensors representing the perception layer, ADC-Raspberry Pi-Cloud connection represents the network layer. The data processing layer is the cloud based ThingSpeak platform that is integrated with MATLAB and the application layer is the GUI provided on ThingSpeak for data visualization.

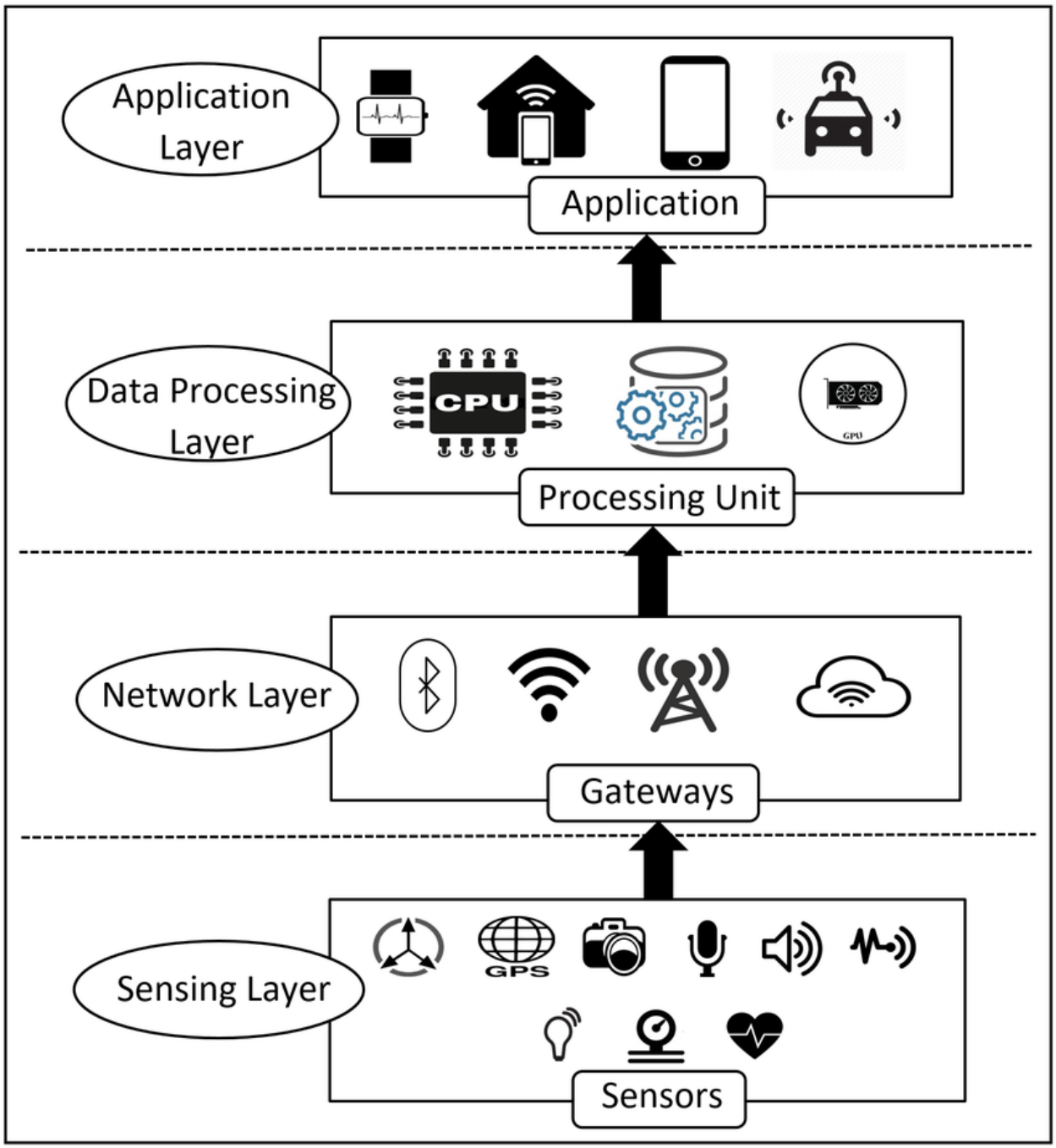


*Fig 2.4. IoT for AMB architecture* [26]

### 2.3.1 IoT Functional Blocks

IoT consists of important functional blocks that facilitate the implementation of its goals such as sensing, actuation, identification, management and communication. The blocks include:

- **Device:** These are the smart objects which make up the main part of IoT, and they can perform the sensing, actuation, control, and monitoring tasks [27]. The devices have interfaces that enable data exchange with other devices as shown in Fig 2.5.

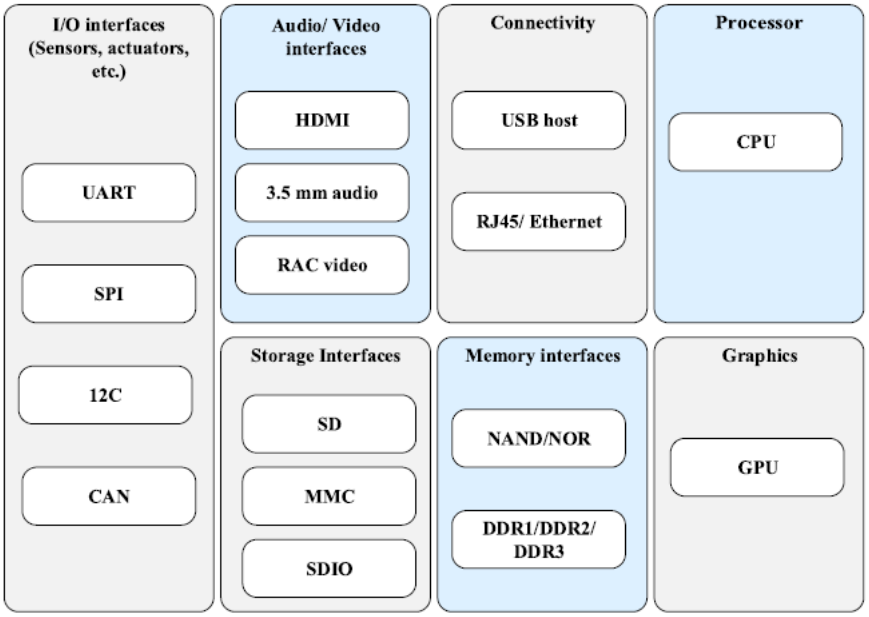


*Fig 2.5 IoT device components* [27]

- **Service**: IoT can be used to offer several services ranging from office and home automation, manufacturing, supply chain and logistics monitoring etc. The IoT services can be classified into Identification service, service for device, information aggregation, device control, data analytics and publishing to mention a few.

- **Management**: IoT offers unique capabilities of performing management and control by means of virtual and remote monitoring where you don't need to push mechanical buttons and switches. Also, availability of data that enables data-based decision-making to improve performance.
- **Security**: Since IoT involves communication over the internet which can be prone to cyber-attacks and information leakage, IoT systems are implementing many security features like privacy, authorization, authentication, data security, content integrity, and message integrity.
- **Application**: These is where IoT user interacts with an IoT system by monitoring and controlling the connected devices via a user interface on an electronic device such as a smartphone.

### 2.3.2 IoT Enabling Technologies.

#### *2.3.2.1 Sensors and actuators*

Sensors for IoT are devices that convert physical parameters into electrical output signals. They can be either analog or digital. To connect analog sensors to microcontrollers an ADC is required. Currently most sensors are digital and can interfaced with microcontrollers via protocols such as $I^2C$, $SPI, UART$. Actuators on the other hand convert the electrical signals into actual physical output such as motion. Actuators can be electric, pneumatic, hydraulic, or human power. The actuators are customized to produce a desired motion after receiving a control signal from the microcontroller.

#### *2.3.2.2 Communications*

Communication technologies enable IoT devices to link up with each other. The most used communication technologies are Ethernet, Wi-Fi, and Bluetooth. Other technologies common in the IoT world include:

**RFID and NFC** which use radio frequency electromagnetic waves to identify and track unique tags, BLE, which is based on Bluetooth 4.0 standards and meant to work well within similar communication range but using less power [[28].

**Li-Fi** is a new high speed communication technology that transmits data wirelessly using visible light in both directions. Data can be encoded by varying the brightness of an LED bulb at high speeds without affecting the functionality of the light bulb.

**6LowPAN** uses IPv6 communication protocol to transmit data. It's a low-power, low data rate and wireless mesh network based on IEEE 802.15.4 standards [[28]. It has end-to-end IPv6 address nodes and can be easily connected to the internet.

**ZigBee** also is a communication technology based on IEEE 802.15.4 standard which transmits data within a range of 10-100 meters and the devices must be in the line of sight to receive the signal [29]. Commonly used for home automation, network of sensors and medical devices.

**Z-waves** communication technology operates at unlicensed ISM band and is engineered to provide reliable and low-latency transmission within a range of 100 m [28]. The technology is common in-home lights and appliances automation.

**LoRa** is based on LPWAN for bidirectional communications over long distances [30]. Can support secure communications with many devices. Table 2.2 shows the comparison of these different technologies with their range and data rates.

*Table 2.2 Comparison of different communication technologies in IoT* [28].

| | Standard | Frequency | Range | Data Rate |
|---|---|---|---|---|
| Li-Fi | Like 802.11 | $400 - 800\ THz$ | $< 10\ m$ | $< 224\ Gbps$ |
| Wi-Fi | 802.11a/b/g/n/ac | $2.4\ GHz$ & $5\ GHz$ | $\sim 50\ m$ | $< 1\ Gbps$ |
| Cellular | GSM/GPRS/EDGE(2G)<br>UMTS/HSPA(3G)<br>LTE(4G), 5G | $900, 1800, 1900,$ & $2100\ MHz$<br>$2.3, 2.6, 5.25, 26.4,$ & $58.68\ GHz$ | | $< 500\ Kps(2G)$<br>$< 2\ Mbps(3G)$<br>$< 10\ Mbps\ (4G)$<br>$< 100 Mbps\ (5G)$ |
| Bluetooth | Bluetooth 4.2 | $2.4\ GHz$ | $50 - 150\ m$ | $1 Mbps$ |
| RFID/NFC | ISO/IEC 18000-3 | $13.56\ MHz$ | $10\ cm$ | $100 - 420\ kbps$ |
| 6LowPAN | RFC6282 | $2.4\ GHz\ and \sim 1\ GHz$ | $< 20\ m$ | $20 - 250 kbps$ |
| ZigBee | ZigBee 3.0 based on IEEE802.15.4 | $2.4 GHz$ | $10 - 100\ m$ | $250\ kbps$ |
| Z-wave | Z-wave Alliance ZAD12837/ITU-T G.9959 | $868.42\ MHz$ & $908.42\ MHz$ | $< 100\ m$ | $< 100\ kbps$ |
| LoRa | LoRaWAN | $868\ MHz$ & $915\ MHz$ | $< 15\ km$ | $0.3 - 50\ kbps$ |

#### *2.3.2.3 Protocols*

The protocols are the set of rules that outline the syntax, semantics, and synchronization of communication. IoT devices have a wide range of protocols they can use to communicate. The following are the frequently used:

**HTTP:** This is the communication protocol that supports the world wide web (WWW). It's based-on client-server architecture where the client makes a request to the server and the server gives a response [31]. It used transport control protocol for reliable connection. This communication is facilitated without a maintained connection between the server and the client.

**WebSocket**: this communication protocol is purposefully for web browsers and web servers and provides full duplex communication and unlike HTTP, it maintains connection between the client and the server.

**MQTT**: this communication protocol is a machine-to-machine protocol based on publisher-subscriber architecture. The publisher published data on a server (broker) and the subscriber subscribes to the server to receive the data [[31].

**CoAP**: Is used for a special case of constrained IoT devices that have limited computing power, power intake, and connectivity. Similar model as the HTTP request-response model but uses UDP (user datagram protocol) instead of TCP [28].

**XMPP**: Is an open-source standard based on XML (Extensible Markup Language) and can provide several services including real time messaging and collaboration.

**Node-RED**: Is a web based graphical programming tool that enables connection of an embedded development board on the internet [28]. Sensor data can be read and displayed directly in a webpage once a board is connected via This protocol. Commands can also be sent from this graphical tool to the board.

#### *2.3.2.4 Platforms*

The platform provides connection between the sensors and data networks proving backend applications that process the sensor data and present it into meaningful information. With the platform sensor data can be monitored, analyzed and displayed. The platform can also be used to control remote devices. The following are some of the common IoT platforms:

- IBM Watson IoT
- Eclipse IoT
- AWS IoT
- Microsoft Azure IoT
- Google Cloud IoT
- ThinWorx
- ThingSpeak

This research utilized $I^2C$ for sensor connection to the IoT gateway since it was the most appropriate and easy connection with less wiring required. The HTTP communication protocol was used for IoT integration. The protocol was used due to its simplicity, free to work with an accessible anywhere around the world. Finally, the ThingSpeak IoT platform was used because it

is an opensource platform that is linked with MATLAB for easy data export and analysis. The platform also provides a graphical user interface to display real time data. The objective of Integrating the AMB to the internet was achieved with minimal cost incurred.

## 2.4 Literature Review

The research of magnetic bearing integration into the internet of things is a recent research area which has not been exhaustively exploited. The advancement on the internet and communication protocols that allow device to device connection, machine to machine connection and machine to device connection a few researchers have attempted to implement this technology into machine elements including AMBs.

In 2017, [32] used BLE to connect an AMB with a user interface on a remote PC to send data from the AMB sensor to the PC. The developed user interface connected the PC to the MSP432 MCU which is a low power, 32-bit ARM cortex microcontroller as shown in Fig 2.6. The AMB real time rotor position could be monitored on the user interface. This approach of remote monitoring is limited by the range of connectivity using BLE technology and rates of data transfer using the same technology.

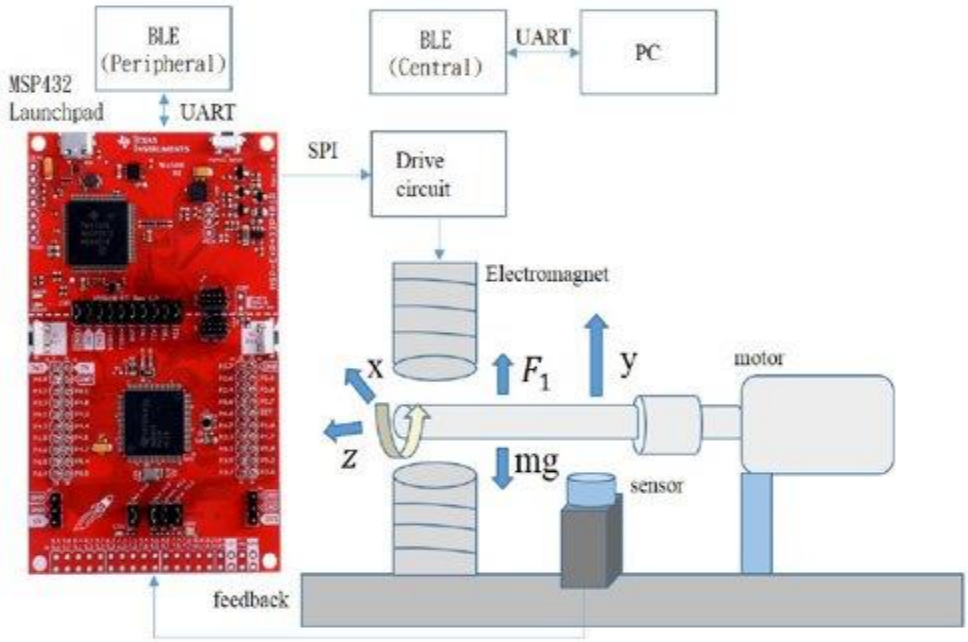


*Fig 2.6. Remote monitoring of AMB using BLE technology* [32]

Real time remote monitoring of a three-phase motor current via the internet was proposed in [33]. The motor was connected to the internet using ESP-8266 WI-FI module interfaced with an Arduino microcontroller. ACS-712 current sensor collected the sensor data and sent the data to ThingSpeak IoT platform where it was remotely monitored as shown in Fig 2.7. The set up was used to monitor industrial motors at a steel mill. The data collected was used to inform the status of the motors during operation. Using the data, system faults or overloading can be detected, and corrective action taken.

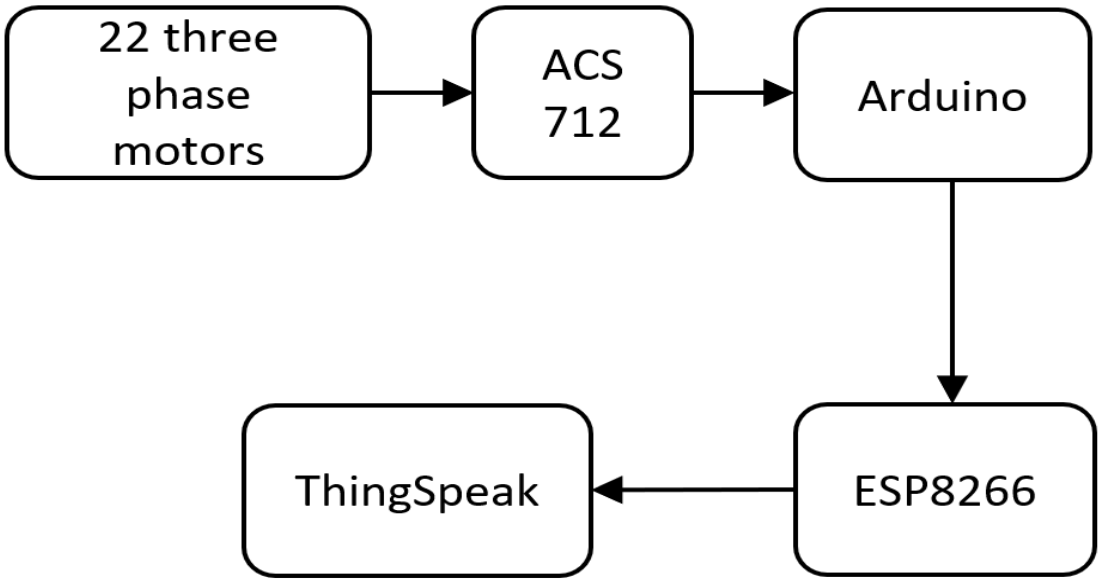


*Fig 2.7. Three phase motor condition monitoring on ThingSpeak IoT platform* [33].

Mamatha & Thejaswi [34] utilized ESP 32 WI-FI supported microcontroller to monitor the voltage, current, vibrations, speed, and temperature of an induction motor. The sensors were connected to the ESP32 microcontroller via the GPIO pins with an ADC interface. The data from the sensors was converted into a digital signal and processed in the microprocessor then displayed in LCD. The LCD was connected to the ESP32 using $I^2c$ bus which reduces the 16 LCD lines to a serial clock and serial data line compatible with GPIO 21 and 22 of the ESP32.

The research focused on the collection of the sensor data from the motor and display it on the LCD and sent to the cloud. Early fault detection can help avert a potential motor failure using the collected data. Additional features such as alert messaging for motor malfunction were also suggested in the research.

Pesch and Scavelli proposed the use of an off-the-shelf IoT gateway to remotely monitor the position and current signal from an AMB [35]. Using the MBC500 AMB test rig they connected the gateway to the AMB via an ADC and a sensor signal amplifier as shown in Fig 2.8. The set up was configured to collect data from the position signal of the AMB rotor in real time and the coil current. The position and current signal were amplified and fed into the ADC to convert into a digital signal since the IoT gateway can only take digital input signals. The IoT gateway had ethernet connection allowing a remote technician to access the sensed data remotely by logging in to the user interface and use the data to diagnose equipment fault or malfunction.

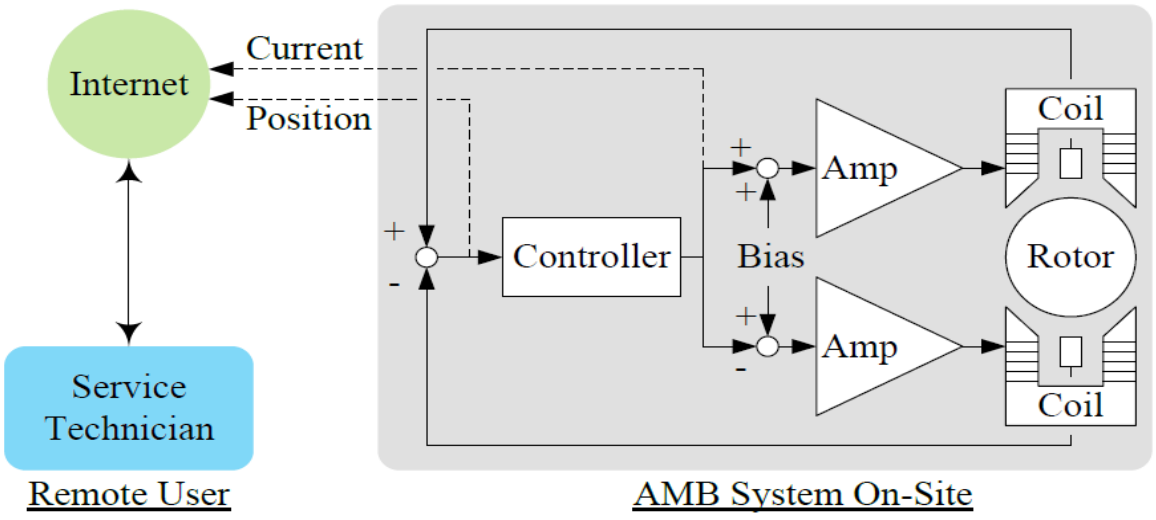


*Fig 2.8. Condition Monitoring of AMB system IoT concept* [35]

A custom remote monitoring software was developed. The software would take the digital data in bits from the gateway and scale it to representative position and current signals using an

offset and sensitivity obtained from sensor calibration. From the position time graph, a FFT was performed to give more insight into the operating conditions of the AMB in the frequency domain. The amplitude-frequency plots interpretation can tell whether there is a fault in the AMB such as rotor imbalance, misalignment and cracks as shown in Fig 2.9 and 2.10. The IoT connection was facilitated by enabling a SSH connection on the gateway. The raspberry Pi gateway hosted a VNC server which could be accessed remotely through the VNC client viewer.

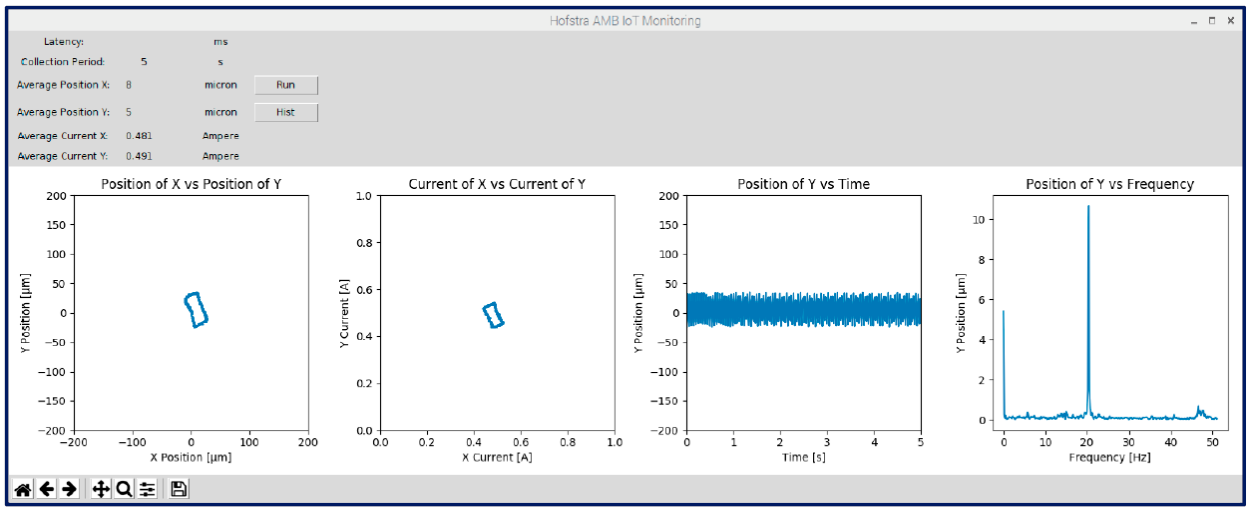


*Fig 2.9. FFT transform of the position time graph of rotating bare shaft* [35]

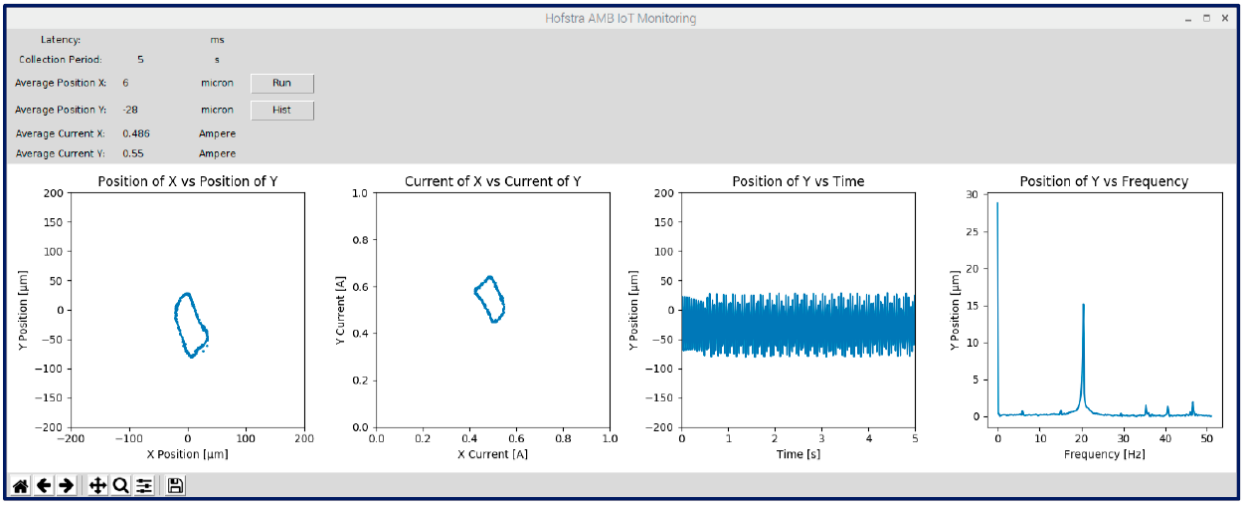


*Fig 2.10. FFT transform of a two balanced collar rotating shaft* [35]

In [36] monitored the motion of the upper limb rehabilitation robot system on IoT. The set up had an upper and lower computer controller. The upper remote computer provided remote interface for a remote user, while the lower computer performed the actual control of the motor drive used in the robotic system. An STM32 microcontroller served as an intermediary between the two computers. Pressure, position and torque sensors were connected to the STM32 microcontroller inputs and the signal from these sensors was processed and sent to the upper remote computer while a command signal form the same STM32 microcontroller went to the lower computer to control the actual motor. The research demonstrated application of IoT in the medical field, but the actual monitoring was focused on the motor which is a rotary machine element like the AMB.

A wireless monitoring architecture for induction motors was demonstrated in [37], using an Arduino microcontroller. The architecture involved a transmission system including sensors,

transducers, and microcontroller, a receiving system and a display as shown in Fig 2.6. Speed, current, voltage and temperature of the induction motors were monitored. A control algorithm in the Arduino was used to control the switching on and off of the motors if a fault or malfunction was detected or switching fans on in case of high temperatures above the threshold. To connect the system to the Internet, a Cayenne cloud system was used in conjunction with Arduino Ethernet shield.

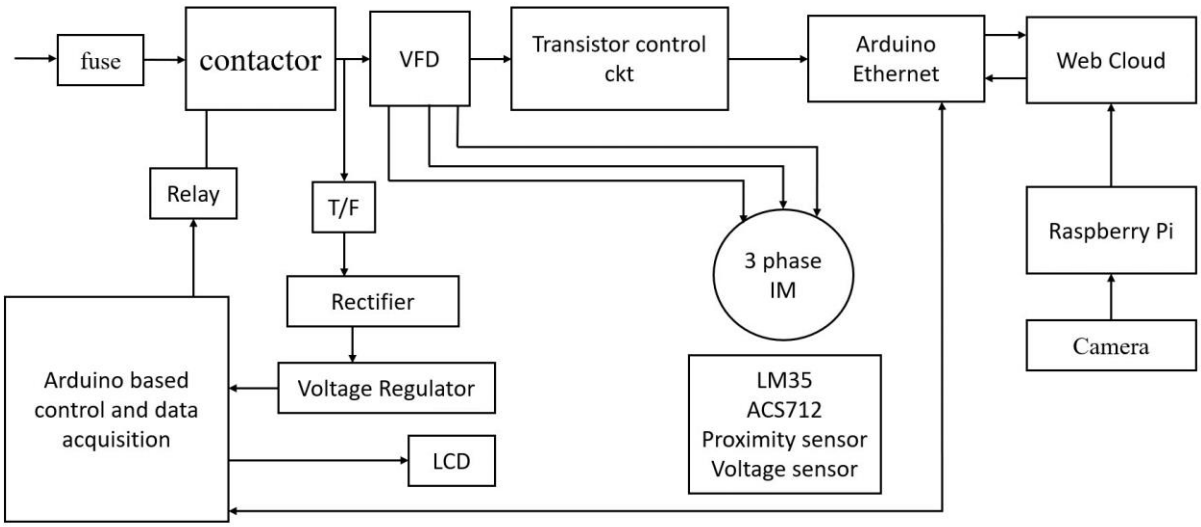


*Fig 2.11. Block diagram of IoT-based monitoring and control system of an IM* [37]

Similar research effort in [38] provides an induction motor remote monitoring on IoT via a Node MCU. The vibrations, speed, voltage, temperature, humidity, and current of the motor were monitored. The data was displayed on a visual basic developed user interface. Fault diagnosis and vibration monitoring of synchronous motor was also demonstrated in [[39] where a web server-database server-client model was utilized.

In most recent developments involving motor and magnetic bearing integration to IoT involved monitoring the imbalance of a rotor by position sensor data and applying SDFT for spectrum analysis to detect motor-bearing fault under high speed [40]. Fig 2.7 demonstrates how the sensor data was acquired from the motor-bearing and through a local industrial computer the data transferred to the internet via MQTT and TLS protocol.

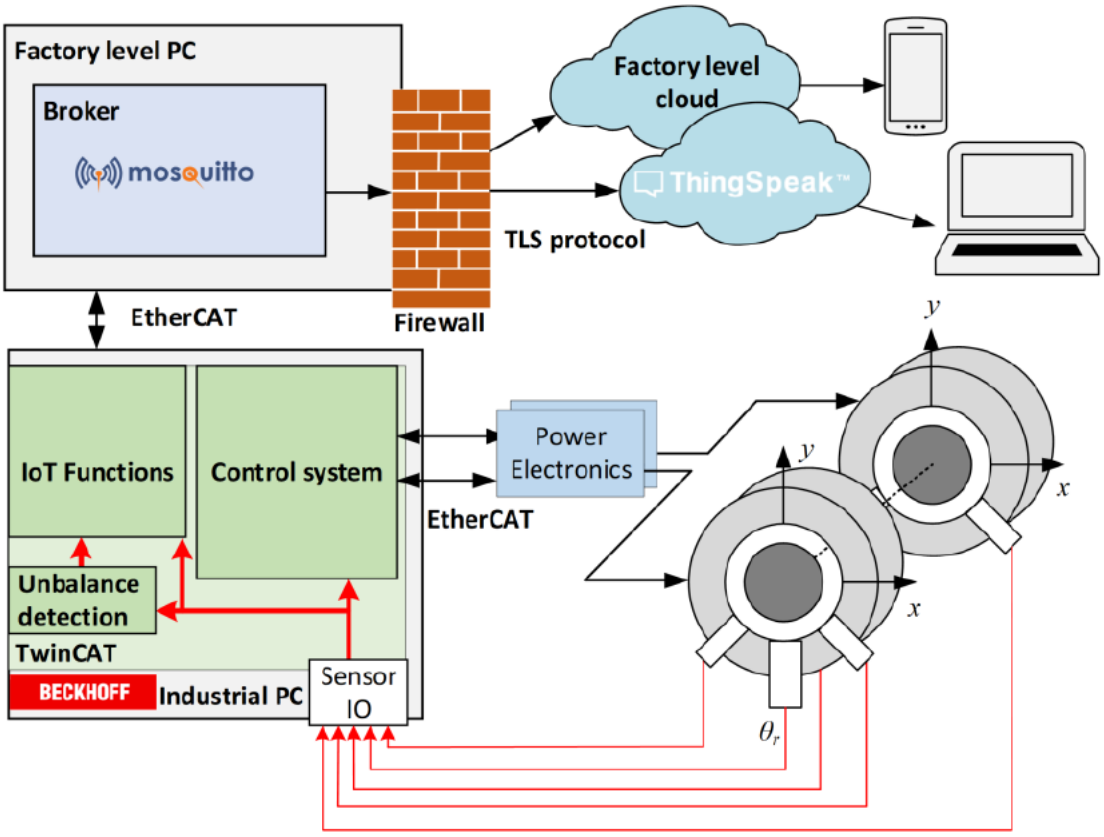


*Fig 2.12. IoT-based monitoring system for a dual motor-AMB system* [40]

## 2.5 Contributions

Previous research has focused on integrating existing current controlled AMBs to the internet for remote monitoring purposefully to collect data and analyze the data. Meaning insights can be obtained from the analyzed data. Little has been done in building an AMB that not only can remotely monitor the condition but also perform remote control to change the state of the AMB.

This research presents a voltage controlled AMB with IoT integration in consideration. The current research leverages on the state-of-the-art digital signal processing technology of pulse width modulation to actively control an active magnetic bearing. This technique enables the implementation of a PID control digitally without the need of having a current control loop, reducing the control loop to just a single loop. By having a single control loop, we have more direct access to the parameters that dictate the dynamics of the AMB, hence better control. The overall components and wiring required for this scheme have significantly reduced as compared to a typical current control scheme.

Furthermore, coupled with a simplified control circuit, the research demonstrates the ability of remotely controlling the voltage controlled AMB, by sending command signals remotely via the internet. A webpage is developed where an authorized person can log in and access the AMB remotely and perform a control action by just a press of a button on a remote computer or a handheld device. The remote control was demonstrated by performing a step response remotely and comparing it with a local step response to evaluate system response.

# 3 AMB EXPERIMENTAL TEST RIG WITH INTEGRATED IoT

In this chapter the steps taken into development of the test rig are shown in Fig 3.1. The sections give a clear outline from the model design, analysis and prototyping of the 1DOF voltage controlled active magnetic bearing test rig. The control algorithm implemented for this AMB was also discussed in this chapter. The strategy for coming up with the controller gains were clearly outlined. The chapter goes into detail on how the AMB was integrated into the Internet-of-Things and how data from the AMB sensors was collected and remote monitoring performed. Furthermore, the AMB was controlled remotely by sending a step response signal which changes the position of the rotor when a request is made online. Finally, the AMB performance was compared while operating using GaN and MOSFET transistors for switching action.

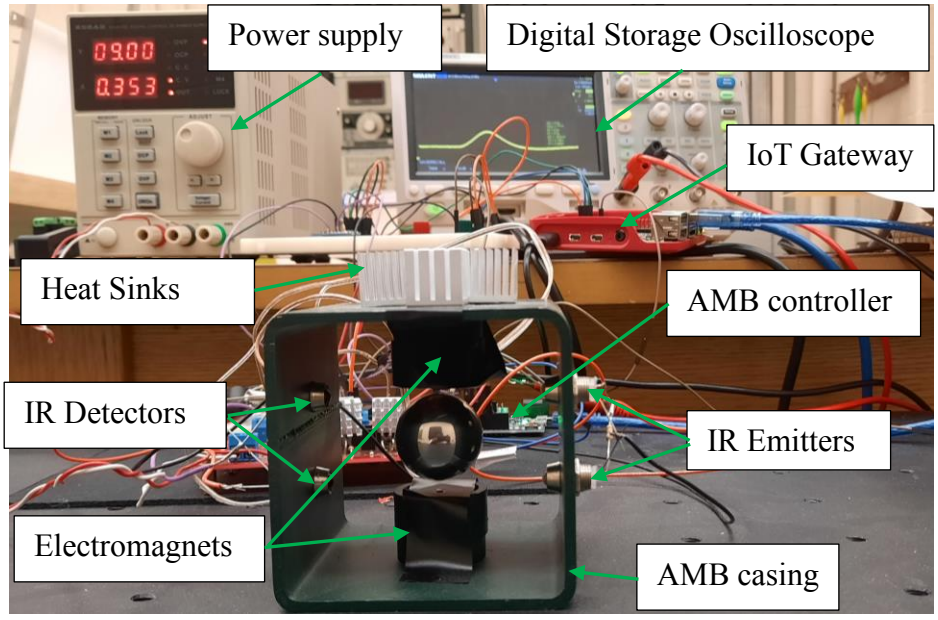


*Fig 3.1. Single axis AMB test rig.*

## 3.1 Overview

The integrated active magnetic bearing test rig is based on a mechanical, electrical, and software system. The mechanical and electrical systems are the physical hardware which form the functional architecture of the AMB. The mechanical system includes steel casing for structural support and positioning of electromagnets, core and ring which house the electromagnetic coil and the levitated mass. The electrical system includes the electromagnetic circuit, the sensory circuit, analog to digital converter, power supply, microcontroller and IoT gateway. The software systems involve an algorithm that performs the control actions, a program that links data from the AMB sensors to IoT gateway, a program that reads and write sensor data from the IoT gateway to the cloud respectively, and a program that sends commands remotely from the cloud to the IoT gateway for active remote control of the AMB. Different communication protocols are used at different levels to facilitate the communication of these devices which are discussed here.

## 3.2 Model of AMB Test Rig

The model of the AMB is a simple single axis magnetic levitation system with two electromagnets on opposing directions, a steel casing with cut outs for sensor connections, bolts, washers and a steel levitation mass. A cross section sketch with dimensions is shown in Fig 3.2.

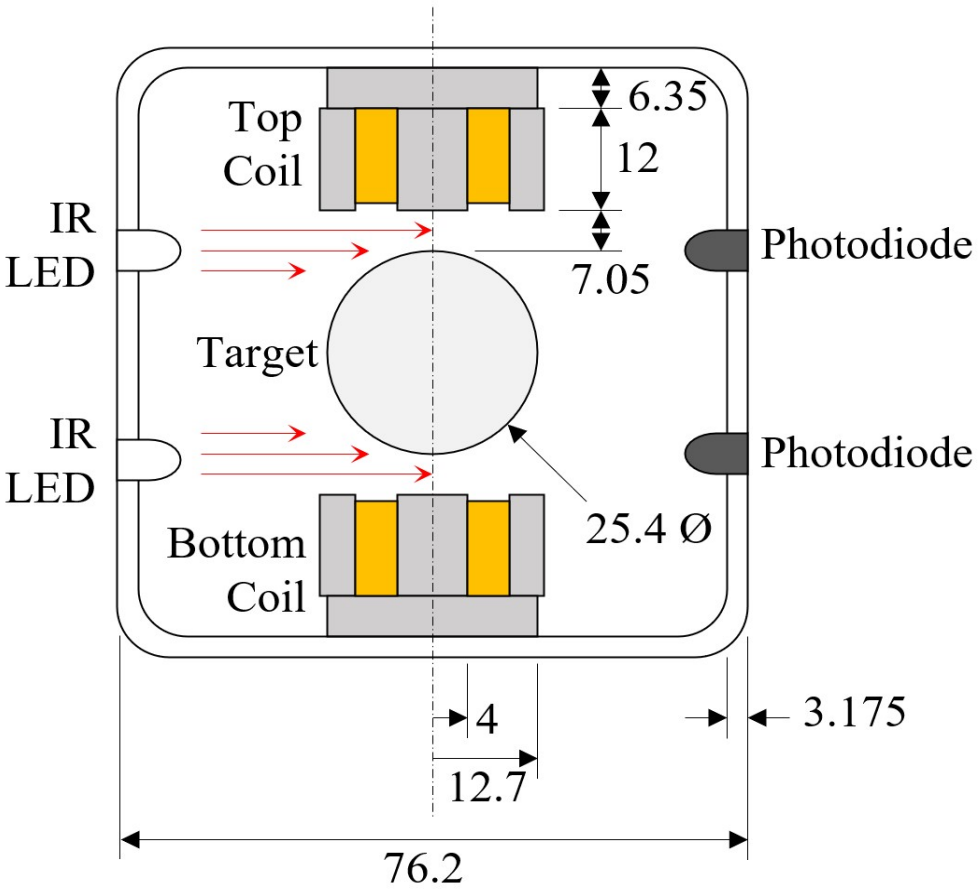


*Fig 3.2. 2D model of the AMB test rig with dimensions in mm.*

### 3.2.1 Steel Casing

The steel casing measures 75 mm by 75 mm by 75 mm. The casing has an opening with an overall thickness of 2.3 mm around the enclosed sides. The casing has two holes drilled on opposite sides and equally spaced vertically for position sensor installation. One side is connected to IR sensor emitters and the other side is connected to IR sensor detectors. The top and bottom sides of the casing also have drilled holes where the two electromagnets are connected. The levitated mass which represents a rotor sits in the middle between the bottom electromagnet and the top

electromagnet. The airgap is controlled by steel washers or spacers that are installed between the casing and the electromagnets. The number of washers can be varied depending on the desired airgap or the number of coils in the electromagnets.

### 3.2.2 Levitated Mass (Rotor)

A spherical steel ball functions as the rotor for the single axis magnetic levitation since the control action focuses on a single axis. The steel ball is 20 grams. The electromagnets generate enough magnetic field force to overcome the weight of the steel ball and sufficiently levitate the mass. The force on each electromagnet varies with respect to the position of the mass in the AMB. The force on each electromagnet is inversely proportional to the square of the airgap. The position of the mass is actively monitored by the position sensors installed on the sides of the AMB. The goal is to maintain the location of the mass within a desired predetermined position with minimal vibrations or variations.

### 3.2.3 Bolts and Washers

Bolts are used to fasten the electromagnets onto the steel casing. Washers with a diameter of 25.28 mm and height of 6.4 mm were added to reduce the airgap. Active magnetic bearings have better control and minimal vibrations when the airgap is small. The bolts and washers also provided additional functionality by helping in confining the magnetic fields within a small area, reducing the magnetic field losses and increasing the overall magnetic force that will be shown with FEA in section 3.8.

### 3.2.4 Steel Rings

Due to leaking magnetic fields initially observed on the finite element analysis, steel rings were added around the electromagnets to help control the field and confine them within the desired area. The steel rings helped to achieve a uniform magnetic field results to a uniform magnetic force experienced by the rotor.

## 3.3 General Electrical Circuitry of Test Rig

The overall circuit diagram is shown in Fig 3.3, including sensor, actuators, and controller. Each sub system will be discussed in turn.

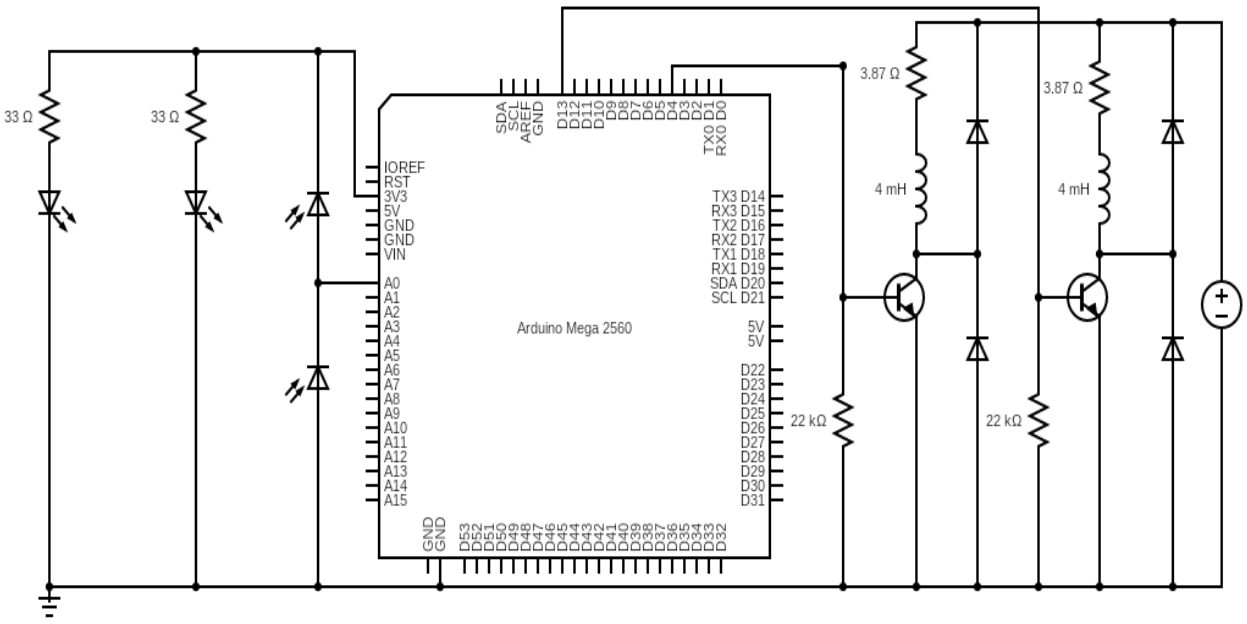


*Fig 3.3. AMB test rig overall circuit diagram.*

### 3.3.1 Infrared Sensors

The infrared (IR) sensors have an emitter which is a light emitting diode and a photodiode detector. The working principle of the IR sensors involves changing the voltage signal in the circuit relative to the amount of infrared light detected. As the position of the rotor keeps changing on the AMB, the amount of IR light detected changes which varies the voltage signal. Essentially, the Voltage signal varies from 0 V to 3.3 V as the rotor moves from the bottom electromagnet to the top electromagnet. The relationship between the signal generated and the position of the rotor can be formulated and used to actively control the position of the rotor. The emitter and the detector are shown in Fig 3.4.

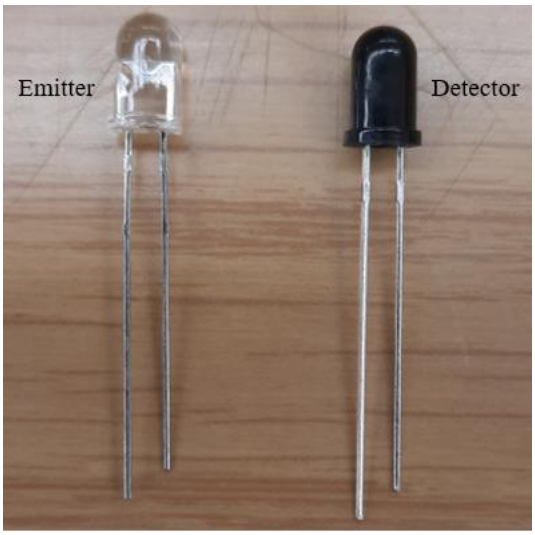


*Fig 3.4. Infrared (IR) emitter and detector.*

### 3.3.2 Two 33 Ω Resistors

To avoid damaging the emitter by the excessive current, each of the two resistors were connected in series with the emitters. The resistors reduce the current going through the emitters to a recommended 50mA ensuring that they function effectively.

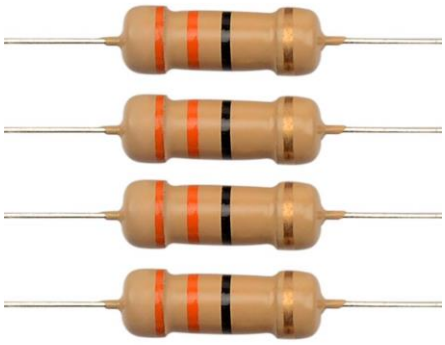

*Fig 3.5. Resistors used in sensor circuit.*

### 3.3.3 Two, Electromagnets

The test rig has two electromagnets with an inductance of 4mH, resistance of 3.87Ω, and 480 coil turns. These electromagnets were selected by calculating the magnetic field force that will be required to sufficiently levitate a rotor weighting 20g as performed by FEMM analysis. The magnetic field force is varied by varying the current supplied to the electromagnet. Although there is a limit to the amount of current that can be supplied to the coils since the wire gauge of 26 AWG was used. The Electromagnets are connected to the top and bottom of the AMB casing where they generate opposing forces to successfully levitate the rotor. The amount of current supplied to each coil is actively regulated by a PWM signal to transistors gates.

### 3.3.4 Two, PHP191 NQ06LT MOSFET transistors

The transistors are the switching elements of the AMB. They help in implementing the PWM signal by the on and off switching action that matches the PWM signal from the controller. The transistors have three pins which include the gate, drain, and source. The drain is connected to the electromagnet, the gate is connected to one of the digital pins on the microcontroller, while the source is grounded. When to signal is low the transistor acts as an open switch while when the signal is high the circuit is closed. The PWM signal controls the opening and closing of the circuit, which controls the average current output to the electromagnets. Fig 3.6 shows the MOSFET transistor used and the symbol.

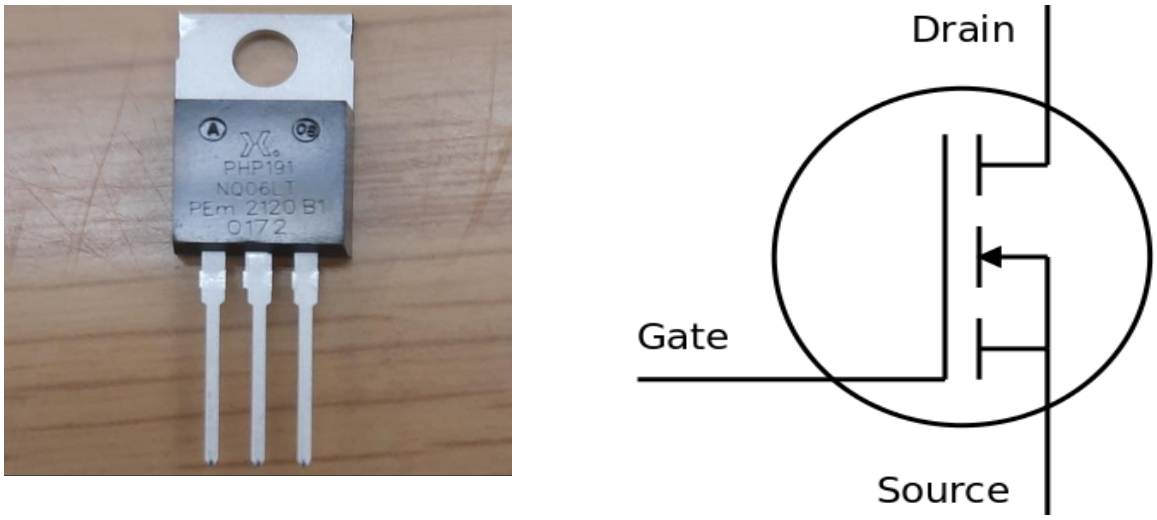


**a)** **b)**

*Fig 3.6. MOSFET transistor, a) PHP 191 NQ06LT MOSFET, and b) MOSFET symbol.*

### 3.3.5 Two, 22 kΩ Resistors

Two pull-down resistors control current flowing to the ground from the digital pins which can cause short circuiting. The pull-down resistors ensure the gate detects the correct signal from the digital pins avoiding any kind of uncertainty between the HIGH and LOW state, avoiding false signal trigger.

### 3.3.6 Four IN4003 diodes

Two diodes are connected in reverse bias to the power supply and parallel to the electromagnetic coils. Each electromagnetic coil has its pair of diodes connected in the same configuration. One diode is connected from the transistor drain pin to the power supply, while the other is connected from the same drain pin to ground. This configuration ensures the residual current flows to ground whenever there is sudden power supply disconnection from the system. Typical diodes are shown in Fig 3.7.

*Fig 3.7. typical diodes used in the AMB application.*

### 3.3.7 Arduino Due Microcontroller

The microcontroller serves as the link between the position sensors and the electromagnets via the transistors. The microcontroller is programmed to implement the PID control algorithm

which utilizes position feedback to perform corrective action. The Arduino takes an analogue signal input from the sensors, performs the control action and outputs a digital control signal through the digital pins to the switching transistors. The analog signal is quantized depending on the bit-size of the microprocessor supported by the microcontrollers. In this experiment a 32-bit ARM Cortex Microprocessor was utilized due to its high resolution in mapping the sensor signal into a digital version for processing. The quantized signal is compared to a preprogrammed set point in the microcontroller and any deviations from the programmed set point generate an error signal which is fed into the PID control algorithm to generate a control signal. The digital control signal in form of a PWM signal is the one that is fed into the transistors via the Arduino's digital pins. Fig 3.8 shows the Arduino due microcontroller used on the test rig.

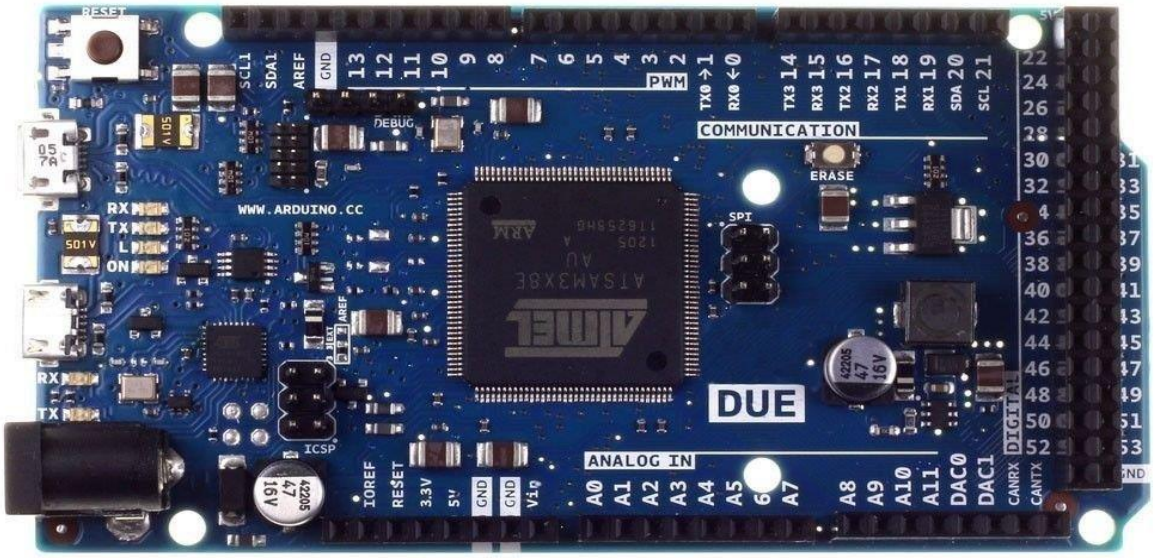


*Fig 3.8. 32-bit ARM Cortex Arduino Due Microcontroller.*

### 3.3.8 9V power supply and 3.3V power supply.

The 9V power supply powers the electromagnets while the 3.3v power supply powers the microcontroller and the IoT gateway. The electromagnets are powered by a Konrad KA3010D benchtop power supply while the sensors are powered by the Arduino Due's power supply pin. The Arduino is powered by USB connection to PC. All have common ground. Also note that this scheme ensures that the sensor signal will never exceed the voltage rating of the microcontroller's analogue inputs.

### 3.3.9 ADS 1115 ADC

The ADS 1115 analogue-to-digital converter (ADC) is a 16-bit sigma-delta ADC with an inbuilt reference voltage, clock oscillator and $I^2C$ interface. The ADC has 4 analog input pins that can be connected to an external device such as an analog sensor. The input signal is compared to the internal reference voltage. The ADC can operate in two modes: single-shot or continuous-conversion mode. Single-shot mode converts the input signal one at a time and stores the converted value to the internal register while the continuous-conversion mode converts the input signal continuously as it receives the signal. The conversion rate depends on the programmed data rate. For this application, continuous-conversion mode was used.

The ADC acts as the bridge between the AMB sensors and the IoT gateway. The ADC takes the analogue signal from the AMB and converts the signals into digital signals that can be read by the IoT gateway. Fig 3.9 shows the 16-bit ADC that was used.

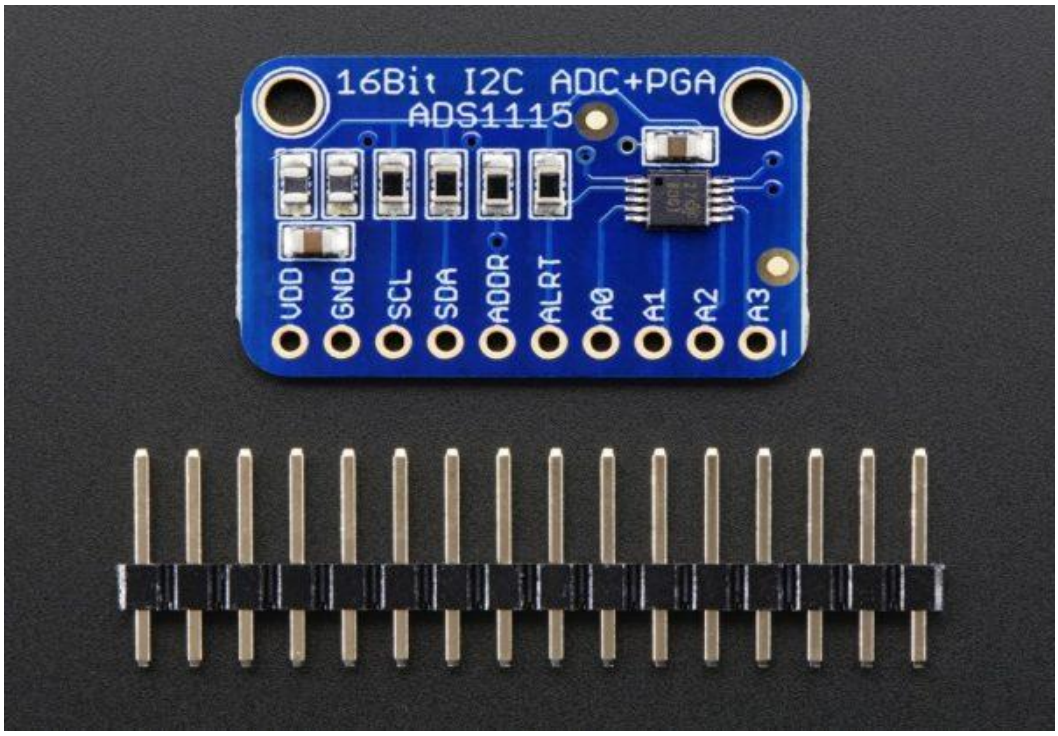


*Fig 3.9. 16-bit sigma-delta ADS 1115 analog-to-digital converter.*

### 3.3.10 Raspberry Pi 4 model B Gateway

The Raspberry Pi 4B is a single board computer and serves as the IoT gateway. The pin out is shown in Fig 3.10. The Raspberry Pi is powered via a 5V USB-C port. The standard GPIO pins can be configured to serve as inputs or outputs. There are designated power pins which include 3.3V and 5V. These pins can be used to power attached peripheral devices. Some standard GP pins support communication protocols such as SPI, UART, PWM and $I^2C$,such as for the ADC.

The Raspberry Pi is programmed to get digital data from the ADC and write the data to a cloud server. The AMB sensors are connected to the Raspberry Pi via the ADC using the $I^2C$ communication protocol. $I^2C$ is a two-wire protocol that connects a master and a slave. Both the

master and the slave can read and write data. One wire called SDA carries data and the other wire called SCL provides the clock signal.

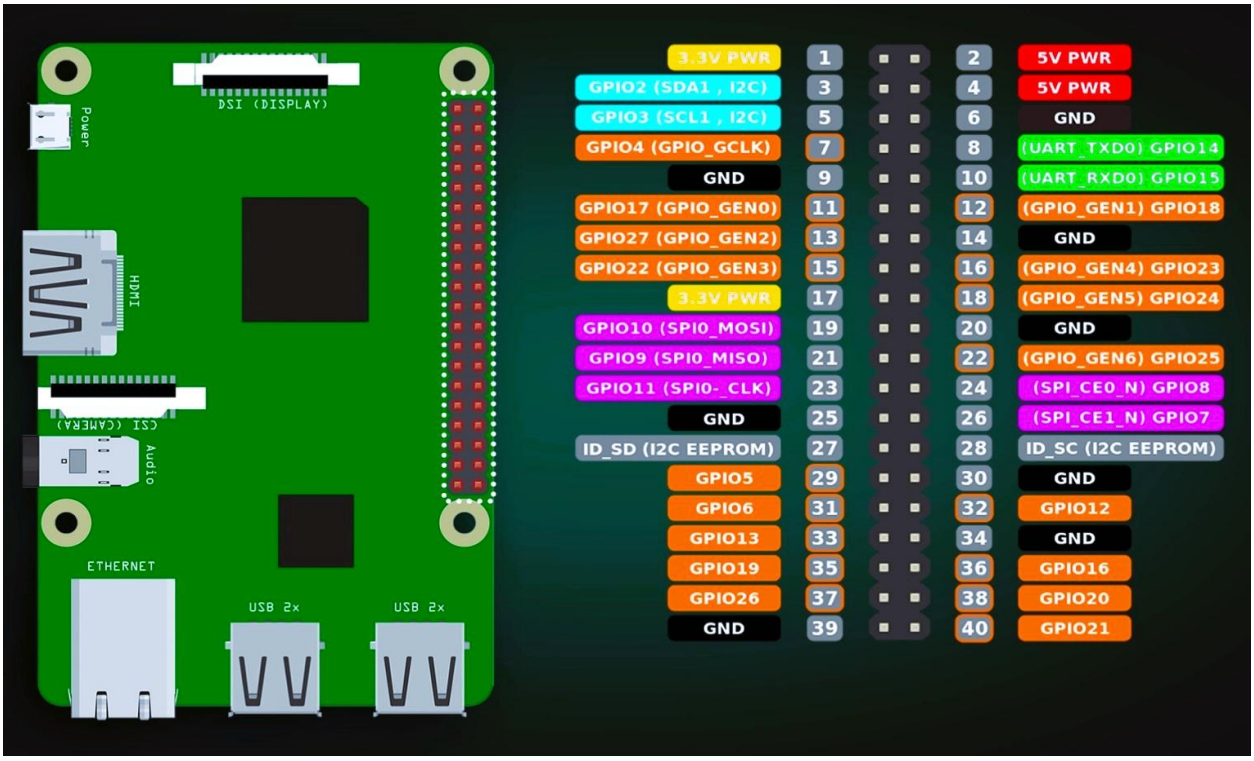


*Fig 3.10. Raspberry Pi 4B with displayed pin out.*

## 3.4 Electromagnetic Circuit

The electromagnetic circuit has an electromagnet whose one end is connected to a 9V power source, and the other end connected to the drain pin of the transistor. The transistor is grounded through the source whereas the gate is connected to the microcontroller which has a pull-down resistor. Each of the two electromagnets has its own transistor circuit that controls the current supplied through each circuit. The top electromagnet transistor drain pin is connected to digital pin 4 of the Arduino microcontroller, while the bottom electromagnet transistor drain pin is connected

to digital pin 13. There are two flyback diodes, one flyback diode is connected in parallel with the electromagnet, and the other is in parallel with the drain-source of the transistor. The magnetic circuit diagram is shown in Fig 3.11.

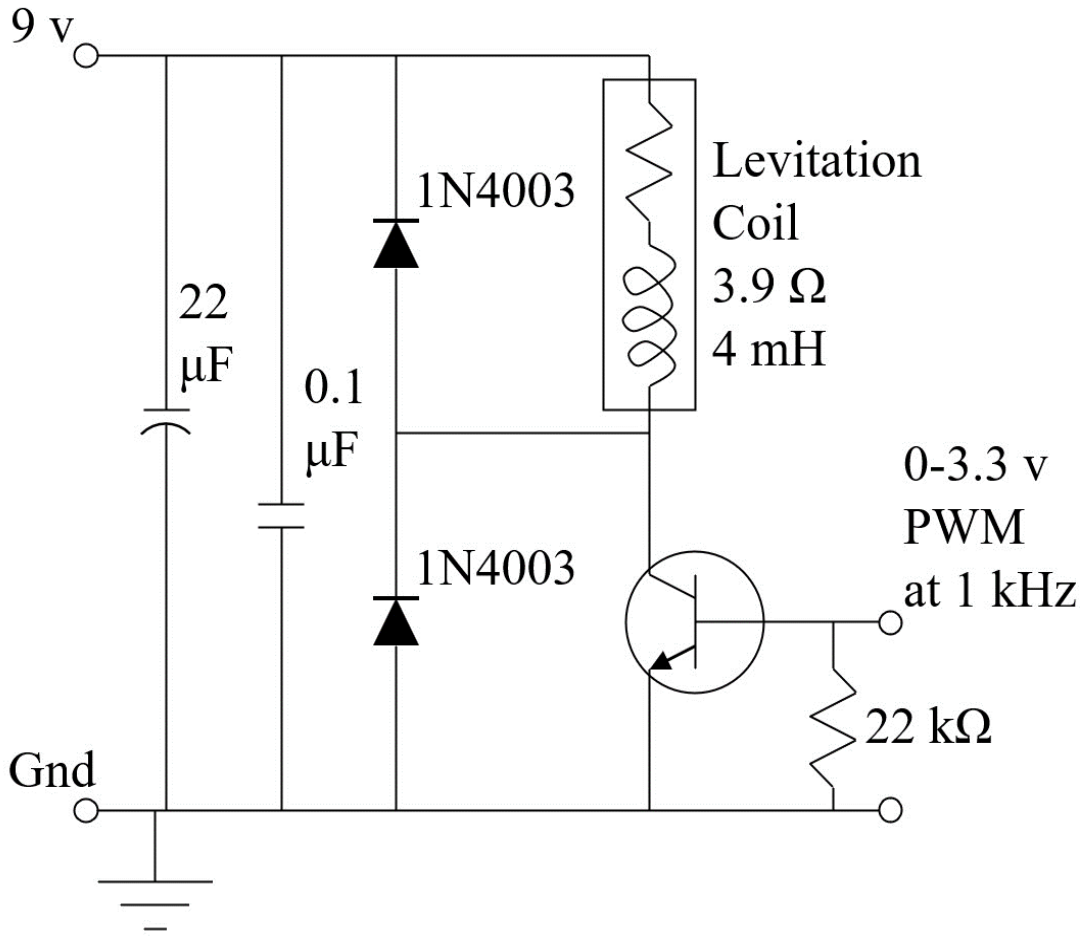


*Fig 3.11. electromagnetic circuit diagram.*

## 3.5 Sensory circuit

The sensor circuit is powered by a 3.3V power supply from the Arduino microcontroller. The IR LED emitters are connected in forward bias with the power supply while the IR photodiode receivers are connected in reverse bias. Each of the two emitter is connected in series with a 33Ω resistor. The emitters are connected in parallel with each other and with the receivers, whose connection is in series. The output signal is tapped between the two photodiode receivers with respect to ground. The sensor circuit is shown in Fig 3.12. The output voltage signal is registered by the microcontroller via an analogue pin on the Arduino board. The signal varies from 0V-3.3V depending on the location of the rotor. The output of the sensors is calibrated with respect to the position of the ball forming a relationship which is used in programming the microcontroller. The calibration curve of the signal with the position of the ball appears to be linear near the operating point (setpoint) of the AMB. Therefore, a linear relationship is used to relate the voltage signal and the position of the rotor. The calibration is shown in the next section.

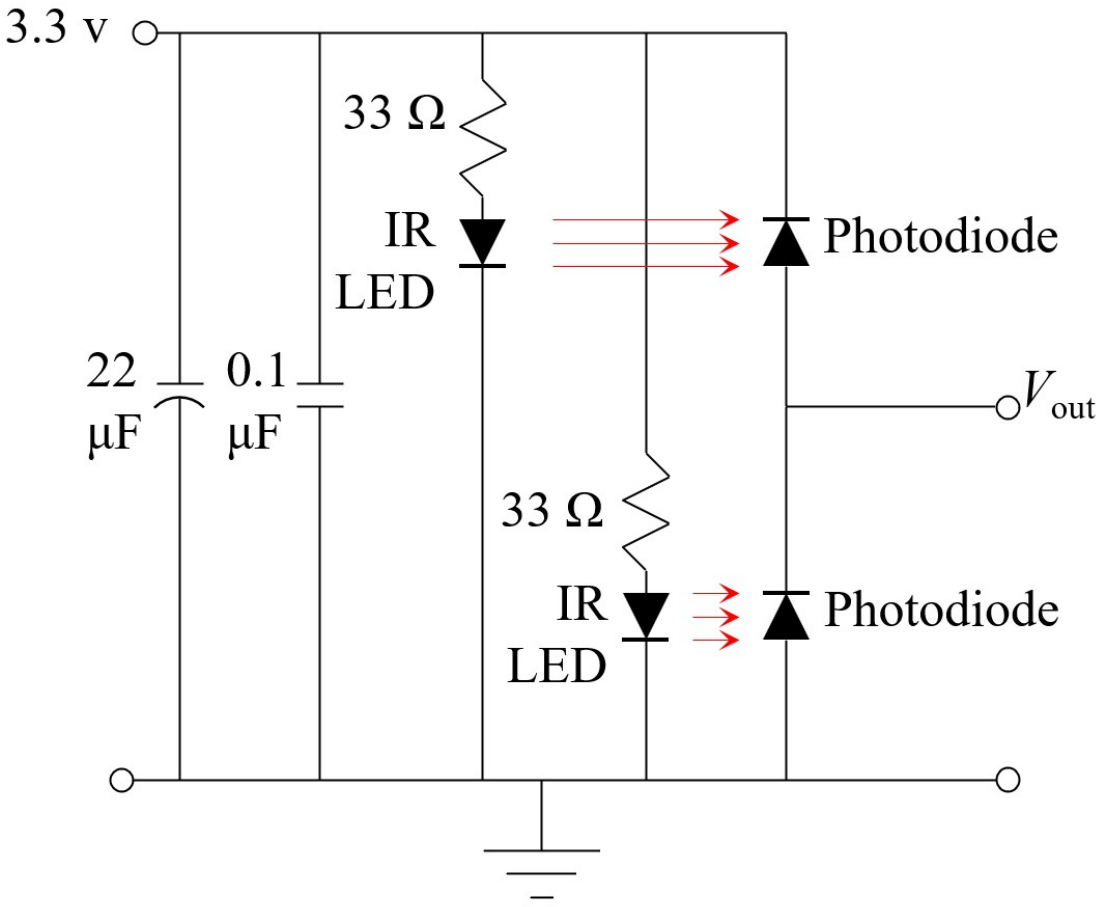


*Fig 3.12. active magnetic bearing sensor circuit.*

## 3.6 Sensor Integration and Calibration

To better control the AMB, sensor calibration is critical. The sensors help in locating the exact position of the rotor, therefore, continuously monitoring the position of the rotor enables corrective control measures to be performed by the controller. The relationship between the rotor position and the sensor signal can be linearized about the operating point.

To set up the AMB for calibration, the rotor was attached to a fixed position. Guide plates we place on the left and right side of the rotor. A steel rule was attached onto one of the guide

plates. The AMB was placed along the guide plates such that the rotor was at a position between the top and bottom electromagnet. The AMB could be slid from a position where the rotor touches the bottom electromagnet to the point where the rotor just touches the top electromagnet along the guide plates. The calibration setup is shown in Fig 3.13.

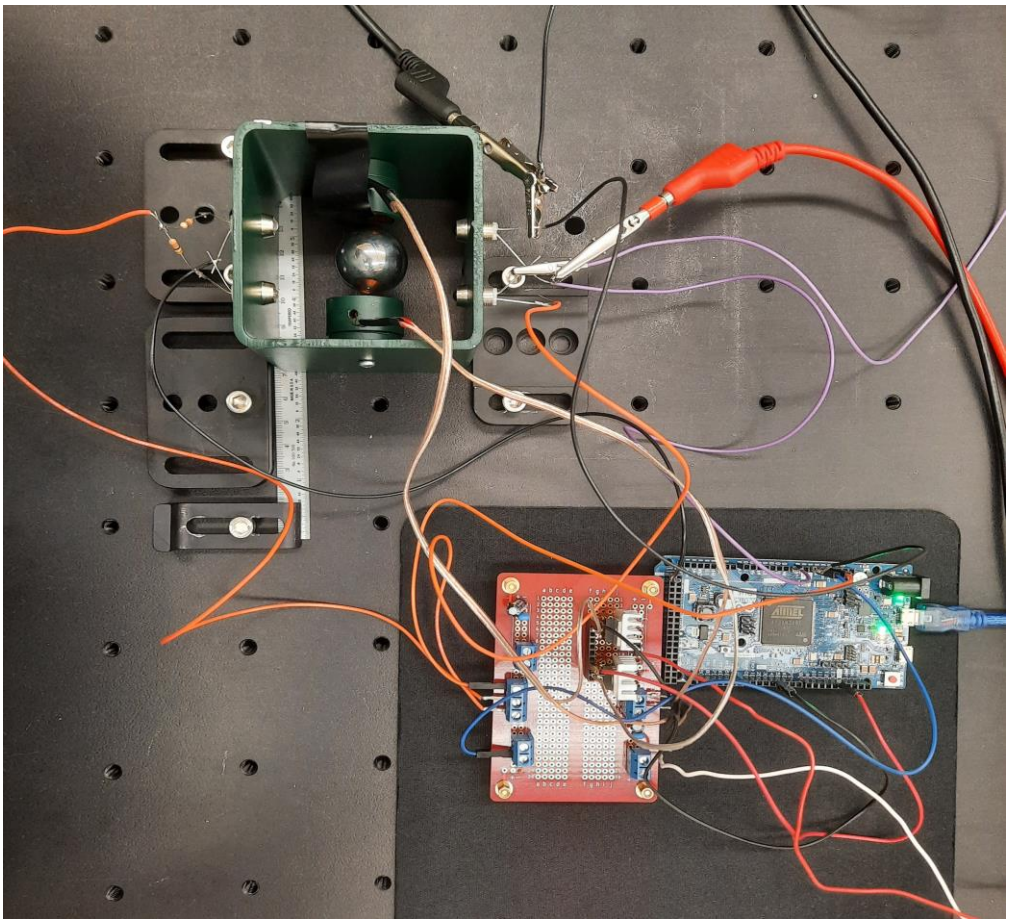

*Fig 3.13. Sensor Calibration set up.*

The sensor output was connected to a digital multimeter to record the output voltage at each position. The AMB was moved at equal intervals of 1 mm apart starting from the position when the rotor just touches the bottom electromagnet, up to the point it touched the top one. At

every interval the output voltage was recorded. The calibration data are shown in Fig 3.14. The output voltage was converted to bits for the purposes of programming the microcontroller. A graph of the rotor position in millimeters vs the output signal in bits was plotted. The output signal at the midpoint rotor position was recorded as the setpoint for the controller. This setpoint served as the reference point for the controller while actively performing the control action where the sensor continuously sends the signal showing the true position of the rotor, the controller compares the received signal with the reference signal and generates a control signal that is fed into the AMB.

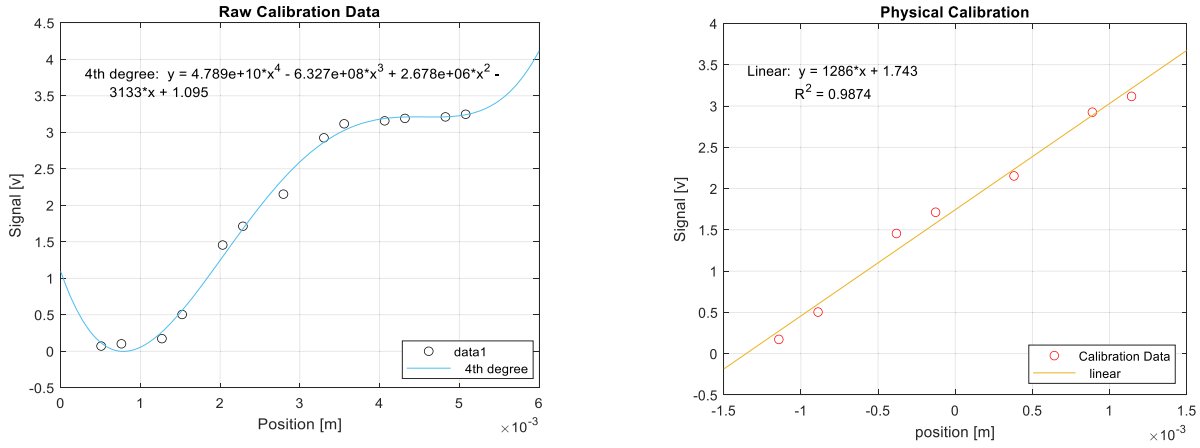


a) b)

*Fig 3.14. Sensor calibration curve, a) Raw data and curve fit, b) Linearized curve.*

## 3.7 ADC-IoT Gateway Circuit

The ADC-IoT gateway connection is facilitated by $I^2C$ communication protocol. The SDA line of the ADC is connected to the SDA line of the IoT gateway, while the ADC SCL is connected to the to the gateway SCL. The connections are illustrated in Fig 3.15. The gateway is powered by a 3.3 V DC power supply through a USB-C port. The IoT gateway acts as the medium linking the

AMB sensors to the cloud platform. The data received from the ADC is translated, aggregated, and processed on the IoT device before it's sent to the cloud. An enabled SSH network protocol protects the data transmitted from the gateway to the cloud.

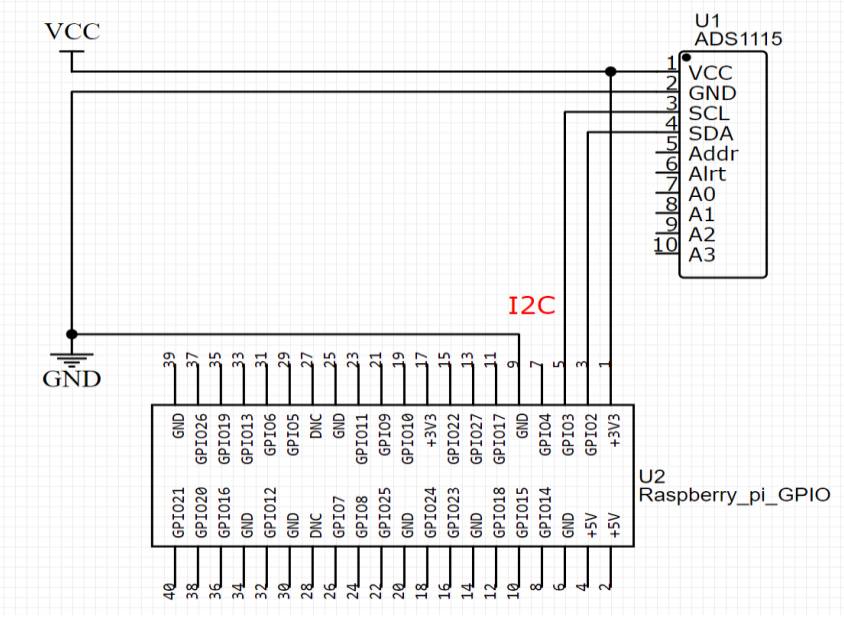


*Fig 3.15. $I^2C$ connection between the Raspberry Pi 4B and the ADS 1115.*

## 3.8 FEMM Analysis for $K_i$ & $K_x$ determination

To characterize and capture the AMB system dynamics, the force-current factor ($K_i$) and the force-displacement factor ($K_x$) are key parameters. Since the AMB exhibits a non-linear system dynamic model, it becomes complicated to analyze the nonlinear model, therefore the nonlinear model is linearized about the operating point. The bearing force generated by the AMB is directly proportional to the square of the current and inversely proportional to the square of the airgap (position between the rotor and the electromagnet). When linearized, the relationship between the current and the airgap is expressed with a constant factor.

The constant factors vary depending on the various parameters of the AMB such as the nominal airgap and the bias current. Therefore, for each AMB the force-current factor and the force-displacement factor must be determined accurately to be able to implement the control of the AMB.

One way to determine the factors was by performing a finite element magnetics analysis. To perform this analysis, a 2D model of the AMB was created on AutoCAD as shown in Fig 3.16 a, the model was exported to a finite element magnetics analysis software (FEMM 4.2) [41]. On the analysis software, the physics of the problem was defined. Each part of the AMB was assigned its respective material and properties. The two electromagnets were assigned the coil gauge wire and the number of coils in each electromagnet.

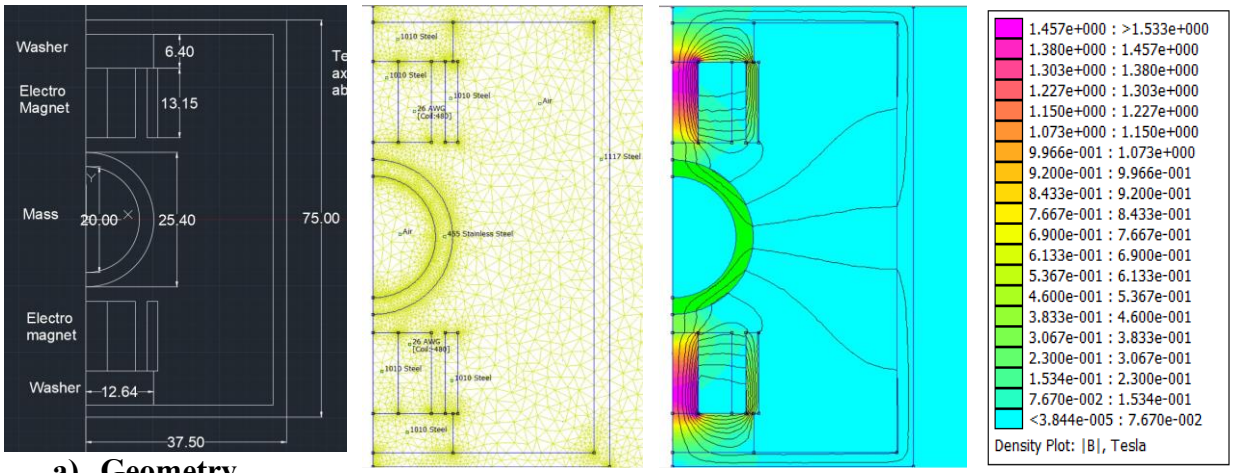


**a) Geometry definition** **b) mesh** **c) Magnetic field** **d) Magnetic flux scale**

*Fig 3.16. Finite element magnetic analysis*

After defining the material properties for each part and boundary conditions, the model was meshed as shown in Fig 3.16 b and solved to determine the force generated. The amount of

current varied from 0 A to 2 A at interval of 0.1 A, the force at every instance was obtained from the analysis. A graph of the force vs the current was plotted. The force-current factor was calculated from this relationship. Similarly, by varying the position of the rotor in the model while keeping the current constant, the force vs the displacement relationship curve is plotted. From this graph the force-displacement factor was obtained. The two constant factors were compared to the factors obtained from the novel experimental procedure used in this research.

## 3.9 Experimental determination of $K_i$ & $K_x$

An experimental method was formulated to determine the force-current factor and the force-displacement factor. The circuit diagram used to measure the electromagnetic forces form the FSR sensor is shown in Fig 3.17. The method utilized a Flexi-force standard ESS301 force resistive sensor (FRS) to measure the force of attraction between the electromagnet and the rotor while in contact. A stand-alone electromagnet with 150 coil turns and 26 AWG wire gauge was used in the setup which is the same as the coils used for levitation. A MCP 6004 op amp amplified the signal from the sensor. A digital multimeter was used for data reading and recording.

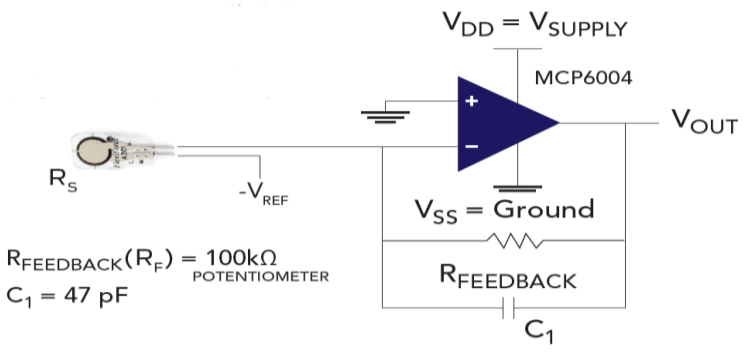


*Fig 3.17. FSR Sensor circuit for magnetic field force measurement.*

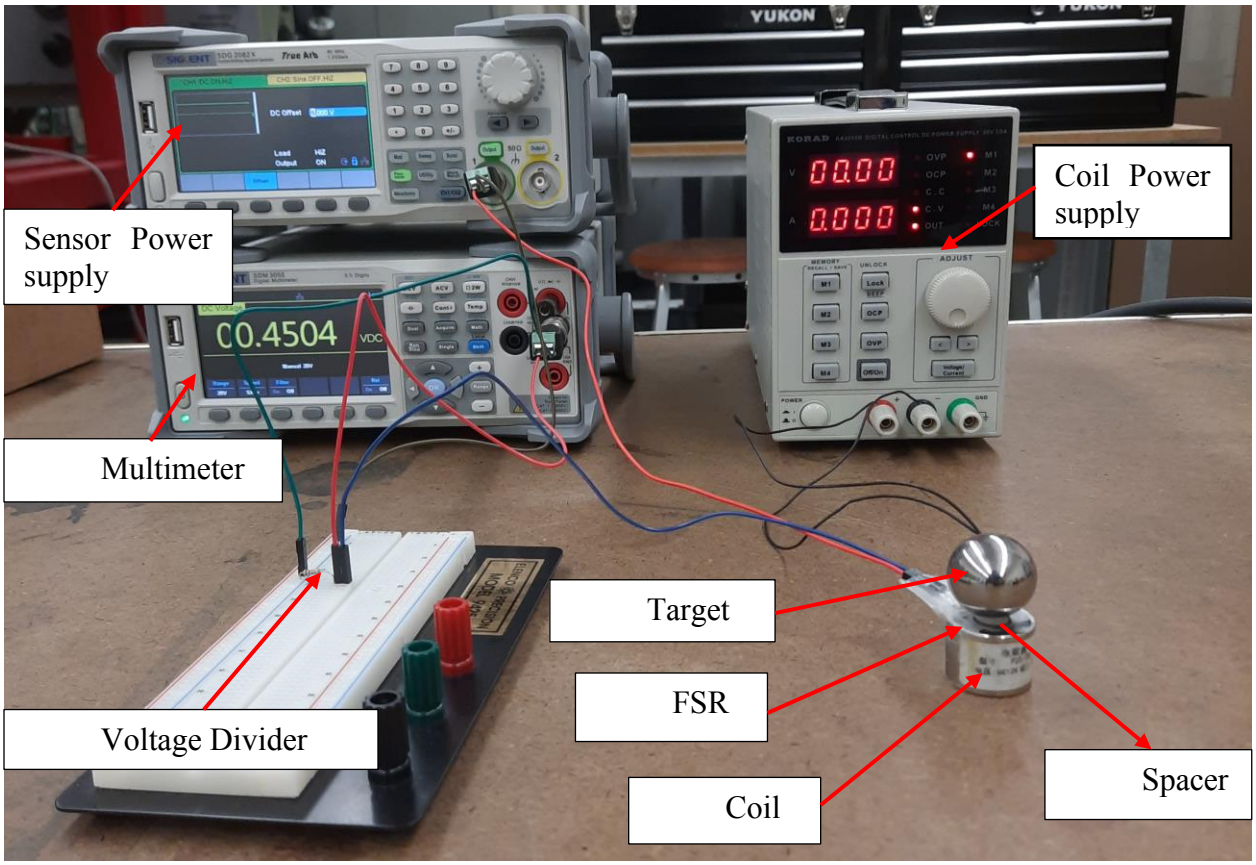


*Fig 3.18. Using FSR sensor to measure the magnetic field force around a mass.*

One line of the sensor was connected to a 6 V power supply, the other line was connected to pin 3 of the op amp. A voltage divider with two resistors in series was connected to pin number 1 and 2 and the ground. The two resistors $R_1$ & $R_2$ values are selected depending on the desired amplification factor required. A feedback resistor measuring $100k\Omega$ and a $47pF$ capacitor was connected between the signal line and the ground in a parallel configuration. Pin number 1 of the op amp was connected to the digital multimeter to display the amplified signal output, pin 4 was connected to a 6V power supply and pin 12 was grounded. This configuration is shown in Fig 3.18.

To determine the force-current factor, the FRS sensor was attached to the core of the electromagnet. The rotor was placed on top of the sensitive side of the FRS. While in that position, the current supplied to the electromagnet was varied at equal intervals and the output voltage signal was recorded from the digital multimeter. The signal voltage was converted to a force reading from a calibrated curve representing the relationship between the force and the output voltage signal of that specific sensor. From the force current graph, the force-current factor was calculated.

To determine the force-displacement factor, the experimental set up was held in the same position as the previous set up, except that in this case the current was kept at a constant current and the position of the rotor varied using brass washers of 0.55 mm thickness. The output signal was recorded at each interval and converted to an equivalent force. The plotted graph of the force and displacement was used to obtain the force-displacement factor. The experimentally obtained parameters were compared to the analytically obtained ones. The two parameters helped in system identification and modelling. To form a linear model which can be used to simulate a PID controller for the AMB, getting the right values for the two constant factors is important.

## 3.10 Simulink Model of the Test Rig

To determine the system performance, a Simulink model was developed and compared to the experimental AMB model. The model used transfer functions that were mathematically modelled from the physical components of the AMB which include the electromagnets, PID controller, the rotor, which was represented by a free mass system, position sensors and external force disturbances. The Simulink model was modelled to closely match the real system although

not all the system dynamics were able to be captured in this model. A PID controller for the model was tuned to stabilize the system model. The proportional, integral and derivative gain obtained from the Simulink model helped to inform the PID gains for the physical system. A step response obtained from the model was compared to the step response of the physical system. The Simulink model is shown in Fig 3.19.

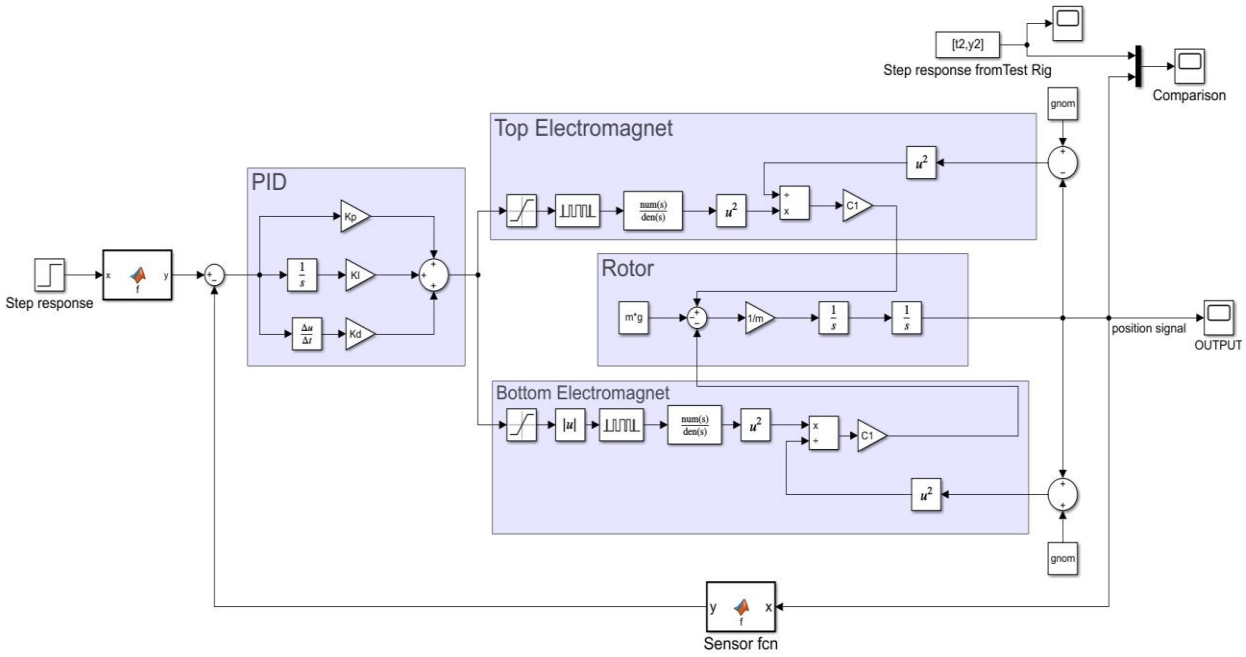


*Fig 3.19. A SIMULINK model of the single axis AMB test rig.*

## 3.11 PID tuning and Experimental Step response

The control algorithm developed for the microcontroller was based on a PID control scheme. With the aid of the model PID control gains, the physical PID gains were manually tuned to establish a stability level where the rotor was able to levitate with minimum vibrations and

deviations from the operating point. The performance characteristics of the system were obtained from a step response.

## 3.12 IoT integration

Integrating an AMB to the internet involved linking the hardware and software using the relevant communication protocols and internet protocols to achieve the goal of remote monitoring and control. The Internet of Things architecture has 4 layers which include the perception layer, the network layer, supporting/data processing layer, and application layer as shown in Fig 3.20. The perception layer is equivalent to a neural terminal which performs the sensing action and collects data from a physical machine. On this research the perception layer includes all the sensors incorporated onto the AMB. The networking layer is the transmission layer that facilitates data transmission from the sensors to the IoT gateway and from the gateway to the cloud. The networking layer provides the data protocols that enable devices to interconnect, communicate and exchange data.

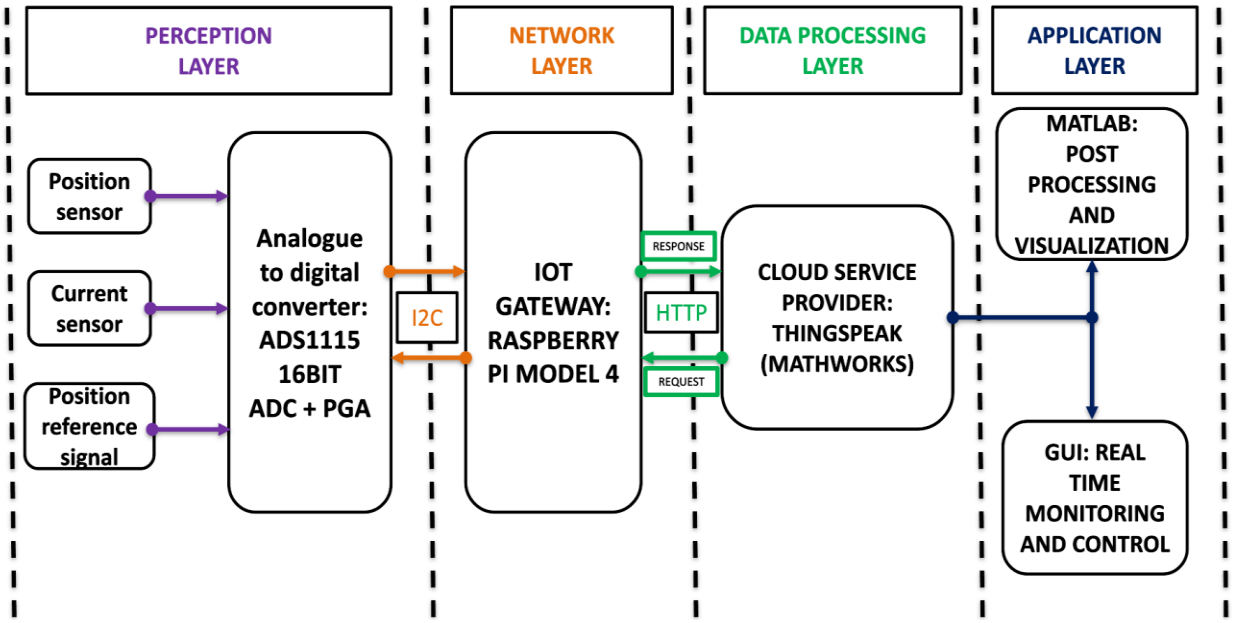


*Fig 3.20. IoT architecture for the test rig AMB.*

The data processing and supporting layer organizes the data collected, filters, and evaluates key characteristics form the data which is provided to the upper layer. This is the layer where the data from the sensors are made into useful information by data management systems and analytical systems such as MATLAB giving insight to the condition of the physical system. From this information, key decisions are made based about the systems. The system can be further remote controlled, if need be, based on the information extracted from the sensor data. The application layer is the uppermost layer which acts as the user interface. It gives a remote operator the ability to remotely visualize the analyzed data and make key decisions from it. The operator is also able to provide commands remotely to change the state of the AMB, for example changing the position of the rotor.

### 3.12.1 Integration of AMB Sensors with ADC

The signal received from the sensors is an analog signal which ranges from 0V to 3.3V. The signal must be converted to a digital signal in order to send it to the IoT gateway. The output signal from the sensors was connected to the ADC via the analogue pins A0, A1 and A2. The ADC ground is connected to the same reference ground as that of the sensors.

### 3.12.2 Linking ADC with IoT Gateway

After converting the sensor signal on the ADC, the digital signal from the ADC was sent to the Raspberry Pi model 4 gateway using the $I^2C$ protocol. The gateway acts as the master and the ADC as the slave. The Raspberry Pi sends a start signal by switching the SDA from high to low and the SCL from high to low. The signal is followed by the address of the ADC. The ADC compares the address sent with its own and if they match, the ADC turns the SDA line high which allows data transmission. Once all the data has been transmitted then Raspberry Pi sends signal indicating that the data was received successfully and accompanied by a stop condition. To continuously receive the data, form the sensors, the Raspberry Pi is programmed to receive the data continuously and feds it into the cloud. This scheme is shown in Fig 3.21.

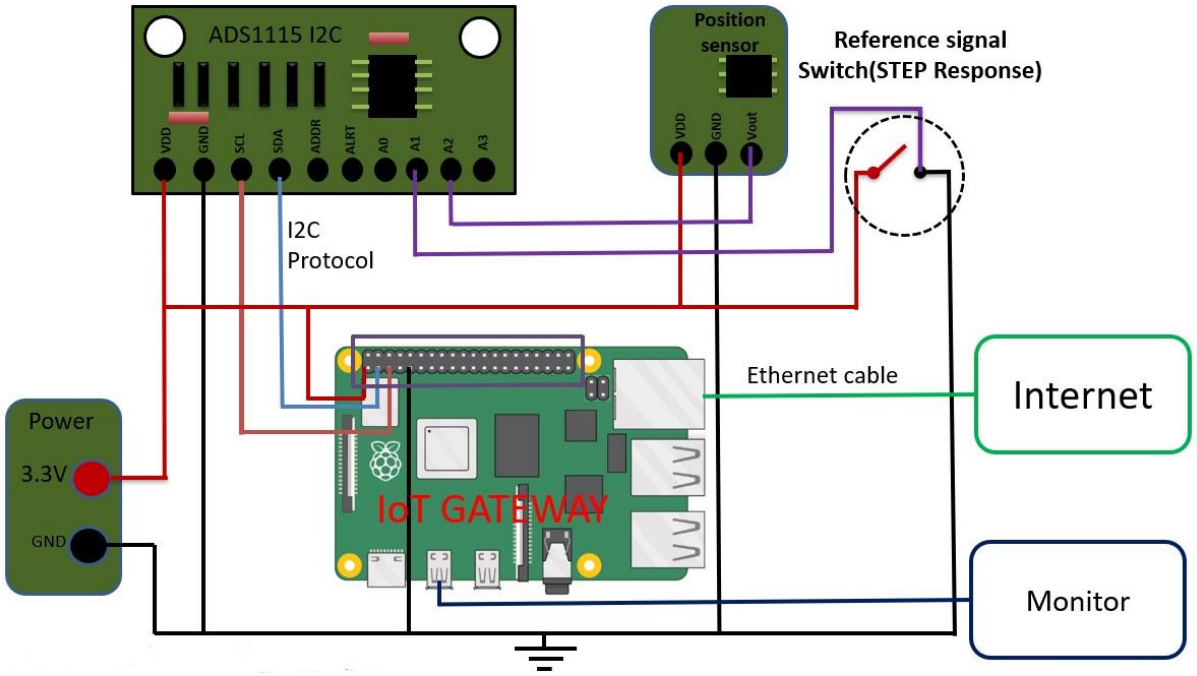


*Fig 3.21. AMB sensor connection to IoT gateway via ADC and linking to the Internet.*

### 3.12.3 Connecting IoT Gateway to the Cloud

An account was created on the IoT cloud platform ThingSpeak. To be able to send data to the cloud platform a channel was created on the IoT platform and named AMB Sensor Data. In the channel three fields were created, one field was to register AMB position data, the second field was to register AMB voltage signal, and the third field was to register the reference signal for perming a step response.

A unique API key was obtained from ThingSpeak. The key was used to program the Raspberry Pi to send data to the right channel over the internet. A Python script was developed to request data from the Raspberry Pi and post the data on the ThingSpeak cloud Platform. The

request program was based on a HTTP protocol which enables exchange of data between the Raspberry Pi and the ThingSpeak cloud platform over the internet.

In this case, the Raspberry Pi was acting as a server and the ThingSpeak cloud platform was the client. The Raspberry Pi subscribes to the server's channel and continuously publishes the sensor data as programmed in the python script. The data received on the ThingSpeak platform was visualized on the GUI provided on the platform. Real time monitoring was possible. The data was update after every one second on the cloud platform.

### 3.12.4 Remote Step Response

One of the main goals of this research was to demonstrate experimentally how AMBs can be controlled remotely. Once the AMB was successfully connected to the internet and sensor data was able to be monitored and accessed remotely, the next step was to set up a remote-control code whose purpose was to send commands from a remote user to the AMB. A typical step response experiment was performed to demonstrate to capability of remote controlling the AMB.

The general flow of the set up was that a web server was developed where a remote user can log in and access the GUI of the AMB. On the GUI the user had a button that they can virtually press to send a command to the AMB. The Raspberry Pi was programmed to read the input commands from the remote user and convert the message into a signal that can control the GPIO pins of the Raspberry Pi. The GPIO pin that was used was set as an output.

The output signal from the Raspberry pi was fed into one of the digital pins of an Arduino microcontroller. Depending on the state of the signal, whether low or high, it invoked a program

in the microcontroller which directly controlled the AMB. The preprogrammed microcontroller then would send a signal to the AMB to perform the step response.

## 3.13 GaNT and MOSFET Comparison for AMBs

The voltage control strategy utilized in this research relies on the switching action of transistors for a better stabilized levitation. The choice of transistor is therefore important in achieving the robustness and stability requirements in the system which dictates the overall performance of the AMB.

# 4 RESULTS & DISCUSSION

The different stages of the AMB development and integration results were demonstrated. The first stage of the development was to identify the custom voltage controlled AMB parameters especially the force current factor and force displacement factor. Two different methods of obtaining these two parameters were considered. The Finite element analysis method and the experimental method.

The force factors obtained from the first stage were used in the second stage in the development of the AMB controller where the system was modelled on MATLAB Simulink. The working principles of the AMB were modelled as transfer functions and a PID controller implemented. By tuning the proportional ($k_p$), derivative ($k_d$), and integral ($k_i$) gains the system performance was established. This SIMULINK model guided the in the tuning and stabilizing of the experimental model where the performance of the ideal model was compared with the performance of the real AMB using a step response.

The third stage was the integration of the AMB to the internet where real time remote monitoring on ThingSpeak IoT platform was performed. The position signal of the AMB was monitored on this platform which could be accessed from anywhere around the world by logging in to the platform and accessing the correct IP address for the AMB gateway. The results of the real time remote monitoring are presented by the interactive user interface on the cloud platform.

The fourth stage of the results present the system response when controlled remotely as compared to when locally controlled. The remote control which was achieved by the

development of a program that would send command signals from a remote device to the IoT gateway and from the IoT gateway to the AMB controller. A website that requires the IP address of the IOT Gateway was developed and used as a remote HMI. Therefore, making it possible to remotely control and simultaneously monitor the AMB response in real time.

## 4.1 FEMM $K_i$ & $K_x$ Results

An important part of designing an AMB is parameter identification. Some of the key parameters to be identified are the ones that control the force dynamics of the AMB. Therefore, part of this research focused on the identification of the force-current and the force-displacement factors since the AMB utilized in the IoT integration was a custom developed AMB utilizing of-the-shelf parts. Table 4.1 shows the key parameter both measured and calculated for the AMB.

*Table 4.1. AMB Parameters*

| Parameter | Description | Value |
|---|---|---|
| $m$ | Levitated mass | 0.02 [kg] |
| $k_i$ | Force-current factor | 0.902 [N/A] |
| $k_x$ | Force-displacement factor | 750.9 [N/m] |
| $L$ | Inductance | $8.85 \times 10^{-3}$ [H] |
| $R$ | Resistance | 3.87 [Ω] |
| $g$ | Nominal airgap | $3.175 \times 10^{-3}$ [m] |
| $N$ | Number of turns | 480 |
| $V_s$ | Supply Voltage | 9 [V] |

The force increases quadratically as the rotor moves closer to the electromagnet. The change is evident when the rotor is close to the electromagnet where a small change in the displacement results in a big change in the force. Although close to the operating point the change is steady with an approximately linear behavior.  making it ideal to linearize the relationship. The slope of this relation was the force displacement factor ($k_x$) in Fig 4.1.a. Similarly, the current and force have a quadratic relationship.

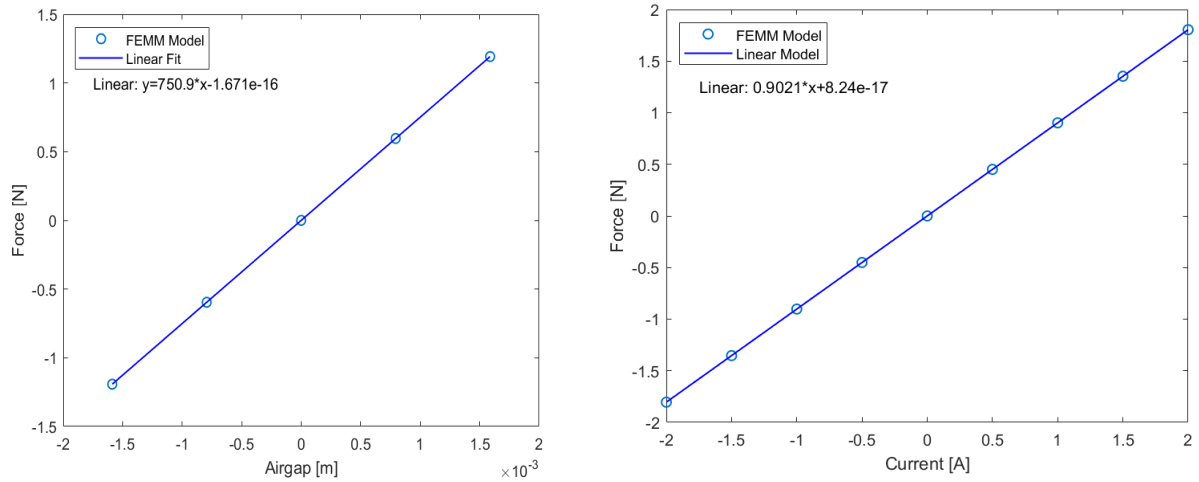


*Figure 4.1. a) Force current factor graph, b) Force displacement factor graph.*

As the current increases the force increases quadratically before reaching the saturation point. The behavior is approximately linear when the current is closer to the bias current since the small changes in current do not contribute significantly to the change in force. Therefore, about the operating point the force current relationship was linearized to obtain the force current factor ($k_i$) as shown in Fig 4.1.b.

## 4.2 Experimental $K_i$ & $K_x$ Results

The force current and force displacement relation was also experimentally measured using FSR sensor and the results presented in a three-dimensional manner where all the three parameters are represented. The analytical computation performed resulted to the graph shown in Fig 4.2.a. which represents the ideal expected force in relation to current and displacement of the AMB. The actual force-current-displacement relationship that was obtained is shown in Fig 4.2.b.

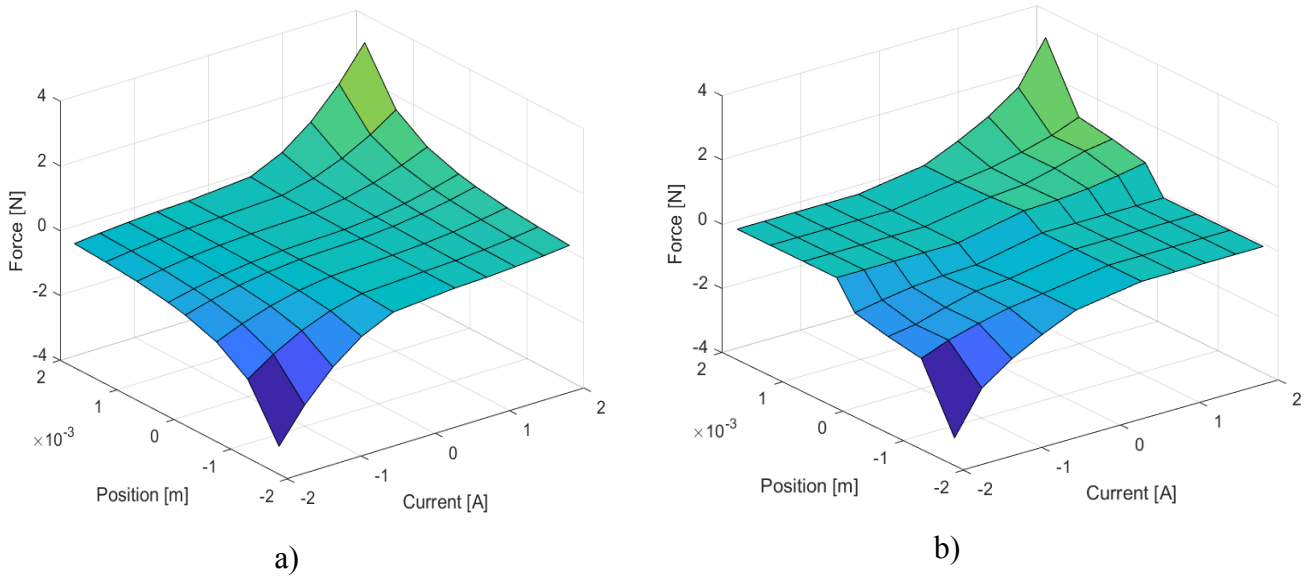


a) b)

*Figure 4.2. a) Analytical force-displacement-current relation, b) Experimental force-position-current relation.*

The Experimental method did not accurately represent the expected electromagnetic force on the mass due to the magnetic field leakage, making it impossible to capture all the magnetic field force generated by the electromagnets. Also, additional contribution of the error resulted from the nature of the sensor used for the force measurement. The Force sensing resistor (FSR) sensors

tend to have hysteresis, non-linearity and drift errors which can contribute to inaccurate force measurement especially when dealing with smaller changes of force.

## 4.3 Simulink Model Step Response and Experimental Step Response

The PID gains were tuned to stabilize the system and a step response was performed to establish the system response. By finding the correct gains of the modelled system, the real system can also be tuned to achieve stability. The system response was compared using a step response from both the model and the real system shown in Fig. 4.3. The setpoint was changed in the microcontroller and the response measured with an oscilloscope. The PID gains, step response parameters were compared in table 4.2.

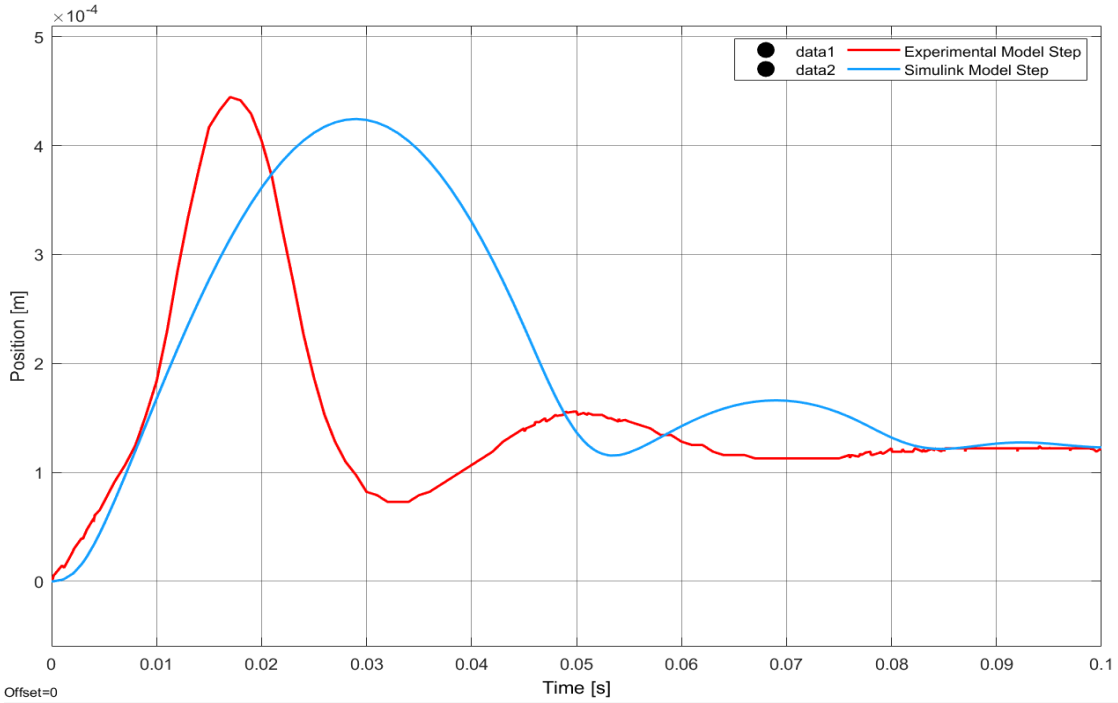


*Figure 4.3. Simulink step response compared with the experimental step response.*

*Table 4.2.PID gains of the Simulink Model.*

| Parameter | Simulink Model |
|---|---|
| Proportional gain $(k_p)$ | $3507.27\ V/m$ |
| Derivative gain $(k_d)$ | $35.07\ Vs/m$ |
| Integral gain $(k_i)$ | $350.73\ V/ms$ |
| Rise time $(T_r)$ | $6.93 \times 10^{-3} s$ |

Tuning the Simulink model PID gains helped in realizing the gains used in the real system. From the step response, the real systems seemed to response faster compared to the simulated model by $0.016\ s$. The real system had a percentage steady state error of 1.13. while the Simulink model had a percentage error of 1.55. The key performance parameters for the two models are shown in table 4.3.

*Table 4.3. Simulink model vs experimental model step response parameters*

| Parameter | Simulink Model | Real System |
|---|---|---|
| Rise time $(T_r)$ | $6.93 \times 10^{-3} s$ | $7.57 \times 10^{-3} s$ |
| Time to peak $(T_p)$ | $0.017\ s$ | $0.026\ s$ |
| Settling time $(T_s)$ | $0.1\ s$ | $0.084\ s$ |
| Final Value (FV) | $1.393 \times 10^{-4}\ v$ | $1.431 \times 10^{-4}\ v$ |
| Steady state error $(e_{ss})$ | $2.22 \times 10^{-6}\ v$ | $1.6 \times 10^{-6}\ v$ |

## 4.4 Cloud Based Data Monitoring and Visualization.

The AMB position was monitored in real-time via the ThingSpeak GUI. On the user interface, three different field were created, the first one was monitoring the actual position of the rotor, the second field was the reference signal for the step response command and the third one

was the PWM signal which represented how the PWM varied with the varying position of the rotor. An example of the GUI for IoT AMB levitation is shown in Fig 4.4.

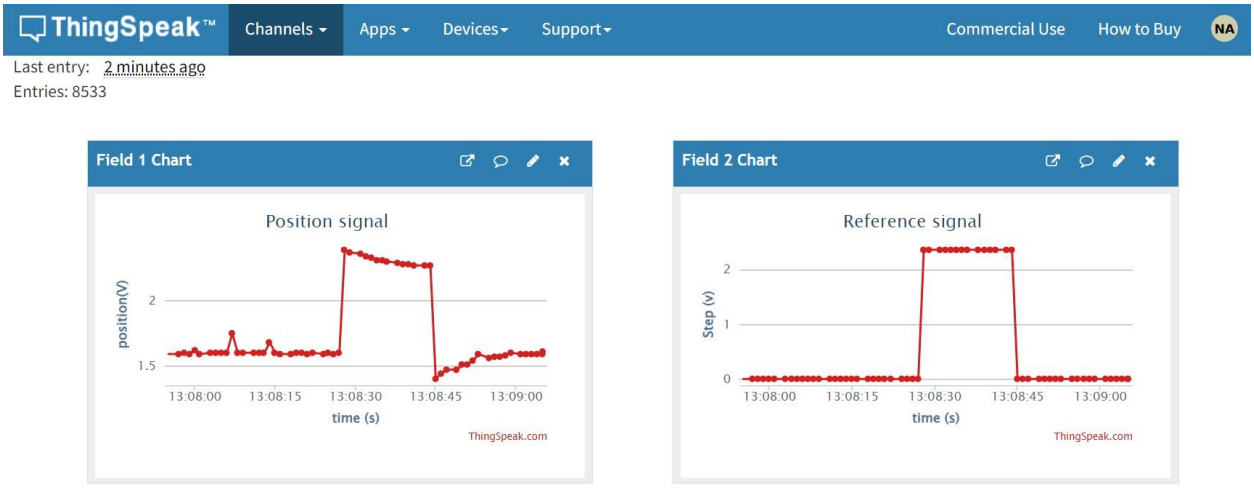


*Figure 4.4. Remote monitoring of AMB rotor position and PWM signal on ThingSpeak Cloud Platform.*

A remote technician can log in to the ThingSpeak platform and actively monitor the condition of the AMB. Equipment with relevant knowledge of rotary systems, the technician can diagnose or identify fault such as imbalance and misalignment. The ThingSpeak platform provides access to MATLAB where data from the AMB can be exported and analyzed to identify intricate faults such as crack identification from vibration data by giving more information about the system.

## 4.5 Local and Remote Step Response

Both responses are measured in the Raspberry Pi, but the remote response is accessed online. The remote step response was successfully performed presenting the possibility of performing other remote-control actions on an AMB. This provides an opportunity to rectify

most common rotor faults such as imbalance and misalignment remotely without the need of physically getting involved. This will significantly reduce machine downtime and reduce cost of maintenance.

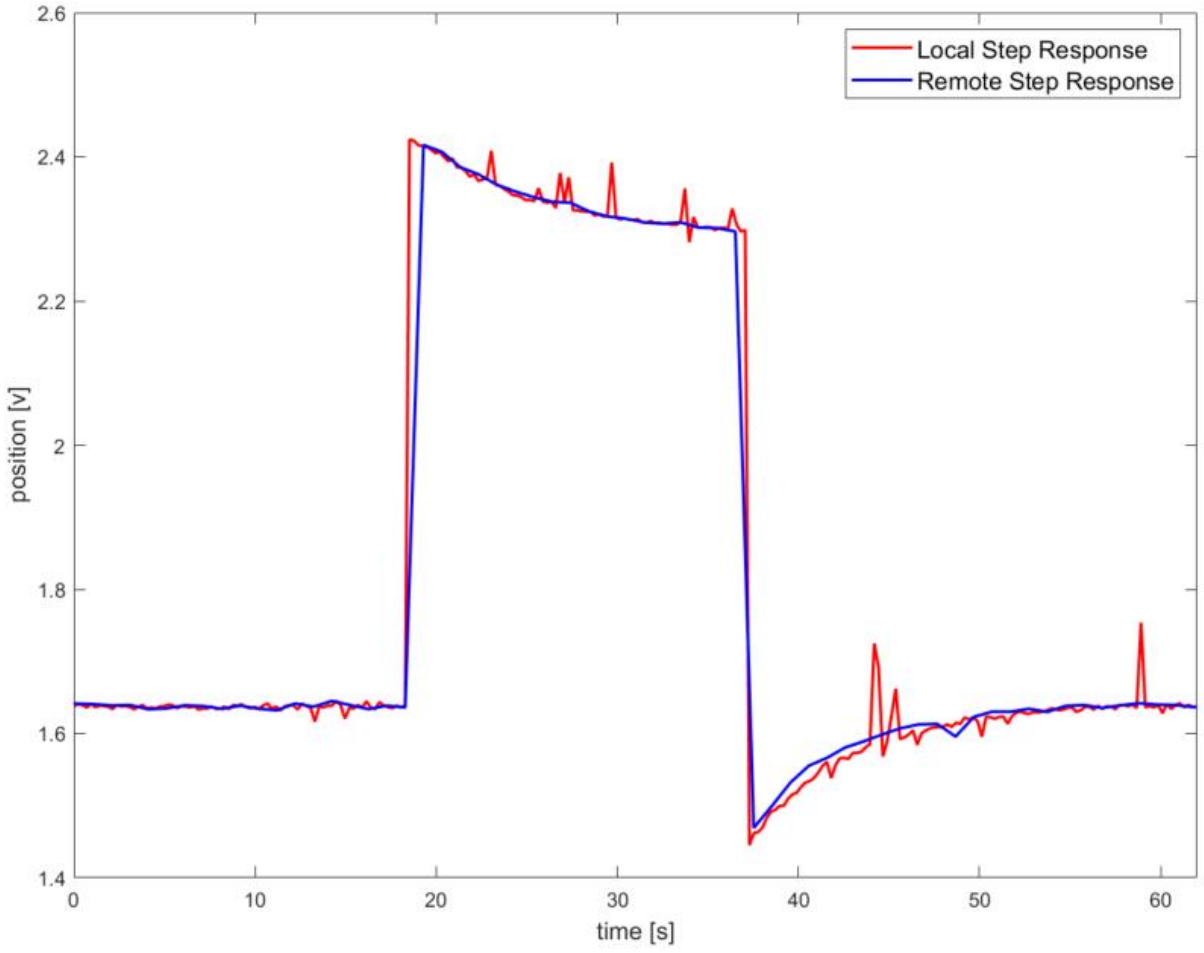


*Figure 4.5. Local step response compared to a remote step response.*

## 4.6 Performance of GaNT vs MOSFET on the Integrated AMB

In a voltage control active magnetic bearing, the transistors used for switching action are important in determining the quality of the levitation. Transistors with a wide band gap and high

switching frequency offers a better performance since the switching takes a shorter time and less energy. Although, other factors such as cost in the industry dictate the preferred transistors for industrial applications. There results were presented from section 4.6.1 to section 4.6.4.

### 4.6.1 MOSFET Switching Action

MOSFET Switching took 0.48 µs from open-to-close as shown in Fig 4.6.a while close-to-open switching took 0.39 µs as shown in Fig 4.6.b. The switching action for MOSFET transistors took longer for both open-to-close and close-to-open switching as compared to GaN.

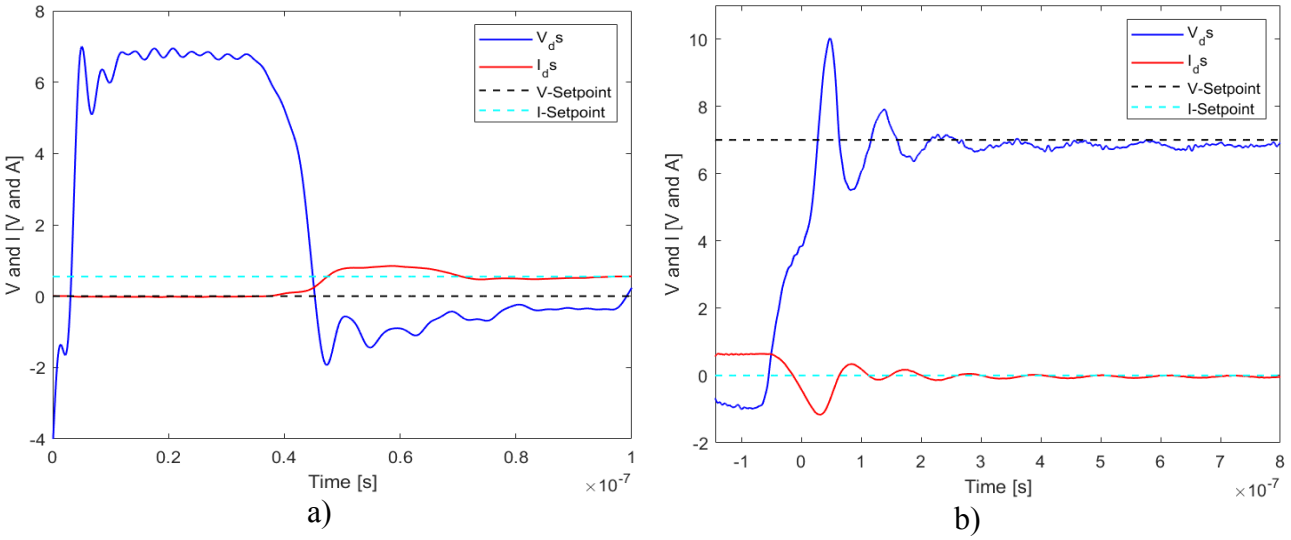


*Figure 4.6. a) MOSFET Switching form open-to-close, b) MOSFET Switching from close-to-open.*

### 4.6.2 MOSFET Power Consumption During Switching.

The power consumption of MOSFET when switching from open-to-close is shown in Fig 4.7.a which amounts to a total energy loss of 0.21µJ. The total energy loss during a close-to-open switching is 3.21 µJ as shown in Fig 4.7.b. The total conductive losses for MOSFET switching are 6.65mW.

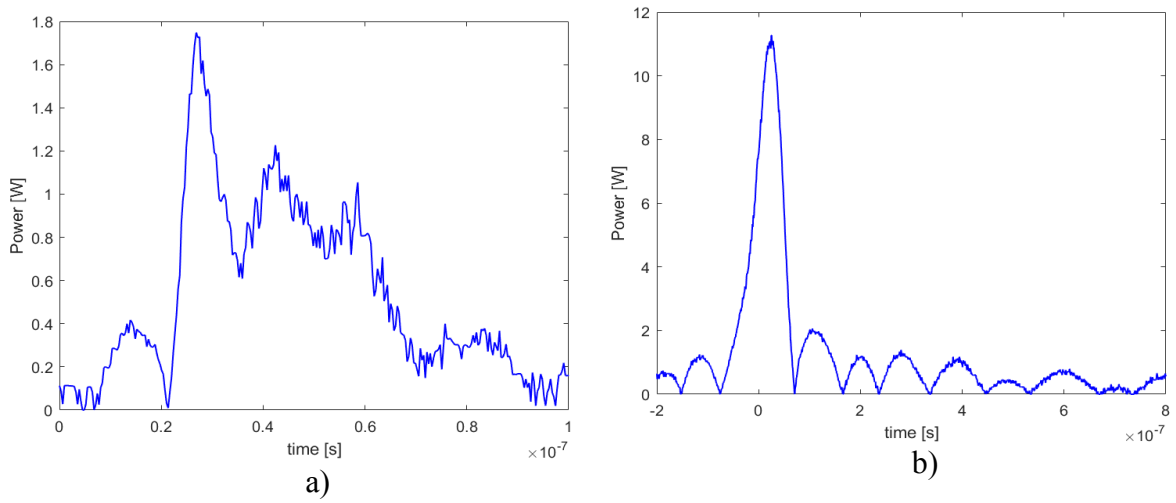


*Figure 4.7. a) MOSFET Power Consumption when switching from open-to-close b) MOSFET power consumption when switching from close-to-open.*

### 4.6.3 GaNT Switching Action.

The switching action of GaNT transistors took 0.17 µs both when switching from open to close and 70.46 ns from close-to-open. The drain-source voltage ($V_{ds}$) and the drain-source current ($I_{ds}$) fluctuation during the switching is shown in Fig 4.8.a & b for open-to-close and close -to-open switching respectively.

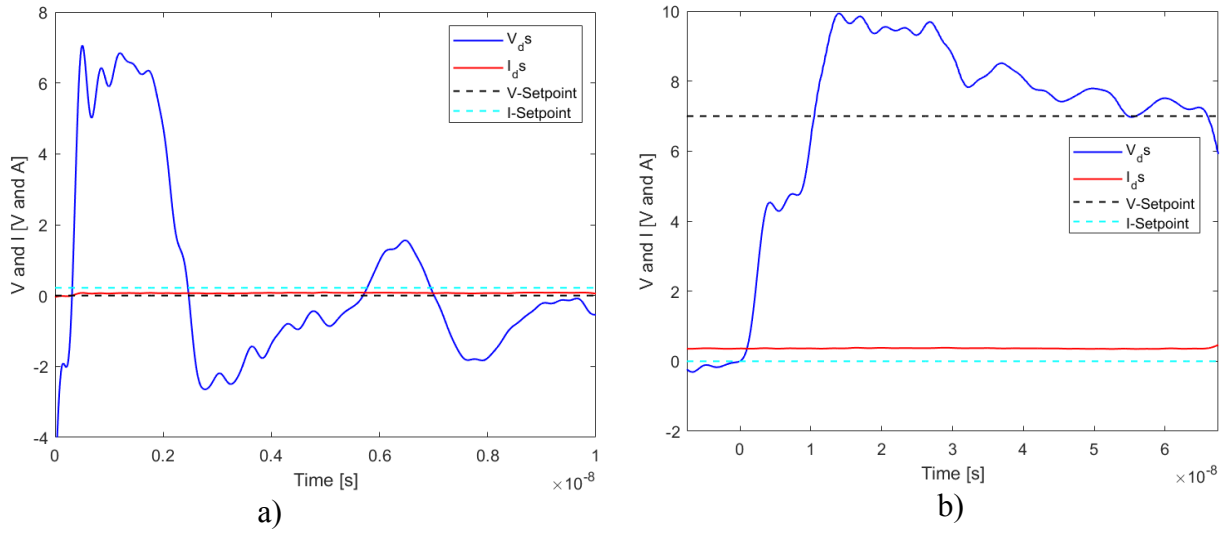


*Figure 4.8. a) Open to close GaN Switching, b) Close to Open GaN Switching.*

### 4.6.4 GaN Power Consumption During Switching.

Switching at a frequency of 1kHz the power consumption from open to close was shown in Fig 4.9.a. The total energy consumed during the switching was 3.29 nJ. Similarly, in Fig 4.9.b. the total energy consumed while switching from close to open was 0.58 µJ. The conductive power loss during the GaN switching amounted to 1.67mW.

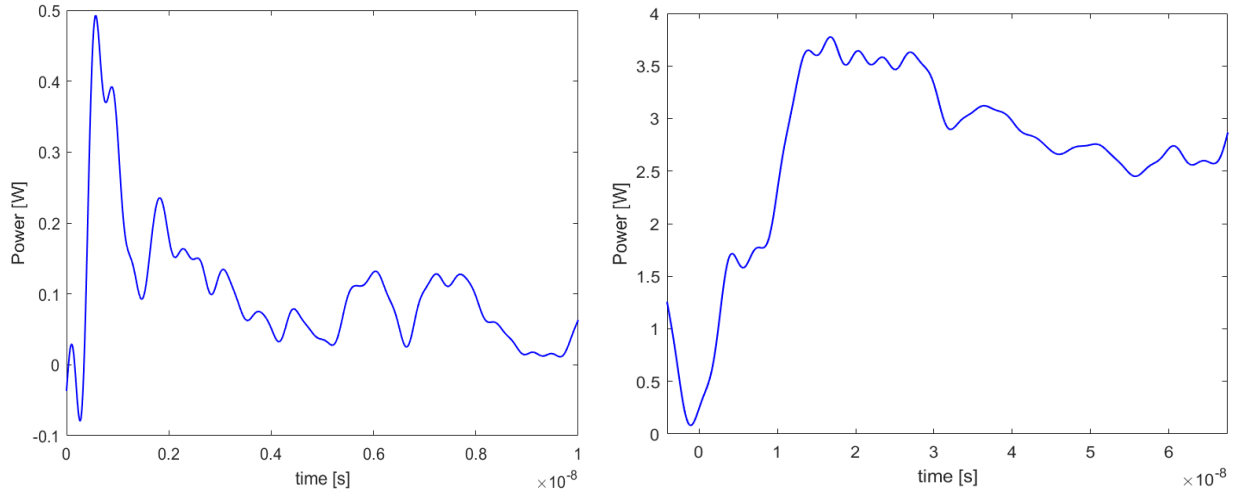


a) b)

*Figure 4.9. a) GaN Power Consumption when switching from open-to-close, b) GaN Power Consumption when switching from close-to-open.*

Therefore, it was found that GaNT provides more efficient levitation in situ than the typical MOSFET. Transistors with a wider bandgap and higher switching frequency such as the GaNs provide a promisingly better performance and can be adopted industrial application of voltage controlled AMB. The overall performance of the two transistors was summarized on table 4.4.

*Table 4.4 Summary of MOSFET VS GaN transistor performance on Voltage Controlled AMB.*

| Measure | MOSFET | GaNT |
|---|---|---|
| Switching losses – close to open | 3.21 µJ | 0.58 µJ |
| Switching losses – open to close | 0.213µJ | 3.287 $n$J |
| Switching time - close to open | 0.392 µs | 70.47 ns |
| Switching time - open to close | 0.48 µs | 0.17 µs |
| Conductive losses | 6.65 mW | 1.67 mW |

# 5 CONCLUSION AND FUTURE WORK

## 5.1 Summary and Conclusion

This research has shown the potential of integrating active magnetic bearings to the internet by opening new possibilities of monitoring and controlling rotating machines. A successful creation of an IoT architecture for AMBs where key parameters are monitored, evaluated and controlled is a clear indication of the progress in the development of smart machines.

The research presented how an IoT integrated AMB can be diagnosed remotely without the need of a technician physically being on site. This was made possible by the real time data from the AMB sensors that was sent to the cloud and through a cloud platform the technician can access, analyze and visualize the data. The presented new way of monitoring machines eliminates the additional logistics involved in performing maintenance. Hence, predictive maintenance is enhanced by having data readily available. The cost of the maintenance procedure is also significantly reduced since one technician can monitor several machines using one computer. The machine downtime is also reduced, which in turn improves productivity of a machine.

The successful performance of a remote step response on the AMB also showed the possibility of controlling AMBs remotely. With the right algorithm, AMB can be remotely controlled by adjusting the rotor position, load balancing, correcting misalignments and imbalances. This basic maintenance procedures can be performed without shutting down the machine. The invention of 5G network also presents a new possibility of implementing the entire control algorithm of the AMB remotely.

## 5.2 Future Research directions

Integrating IoT with AMBs is an emerging area of research that has not been fully exploited. Researchers are actively developing different technologies both in IoT and AMBs which when incorporated together has potential a completely new future for rotating machinery which will in turn change the manufacturing, aerospace and the energy industry. The following areas are key research opportunities that need to be exploited in relation to IoT integration on AMBs:

1. Security and reliability:

   Researchers are working on developing more reliable encrypting and authentication of critical information. Data security is paramount especially if the data is used to controlled machine elements such as AMBs used in power generation or aircraft engine. Also, development of better internet connectivity with built in redundancy will increase the reliability of IoT in critical machine elements.

2. Integration with industry 5.0:

   With advancement of industry 4.0 where automation has taken over the industry, researchers are taking a step further in implementing machines that can make decisions on their own through machine learning techniques utilizing real time data collected overtime. IoT is the center stage in this revolution due to the exchange of data that is required between the machine elements themselves and with the cloud. Successful implementation will Open opportunities for a potential $5^{th}$ industrial revolution.

3. Cyber physical systems and digital twins

   Researchers are working on new concepts of virtualization of physical systems and processes. Physical systems are integrated with intelligent computing systems through a wireless network enabling sensing, actuation, and control. IoT plays a big role in providing the networking infrastructure for these systems.

   Digital twin is also a research concept of creating a virtual model of a physical object. The model is used for simulating the real world and providing feedback which is used to improve the physical model. The two-way dynamic mapping helps real systems to bridge the gap of product life cycle management by learning from the virtual model.

4. Predictive maintenance:

   Real time data collected by IoT integrated systems is used by researchers to develop algorithms that can better predict faults and suggest corrective action before they occur. Data driven predictive maintenance will enhance how industries perform maintenance which will significantly reduce machine downtime, increase reliability and overall reduce the maintenance cost.

5. Regulations and standards:

   With new systems and technology being introduced researchers must partner with regulating authorities to come up with standards and regulations upon which these technologies operate. The regulations and standards will ensure safety and compliance within the emerging industrial segment.

# 6 REFERENCES


[1] G. Schweitzer and E. H. Maslen, *Magnetic bearings: Theory, design, and application to rotating machinery*. Springer Berlin Heidelberg, 2009. doi: 10.1007/978-3-642-00497-1.

[2] A. Tonoli, A. Bonfitto, M. Silvagni, and L. D., "Rotors on Active Magnetic Bearings: Modeling and Control Techniques," in *Advances in Vibration Engineering and Structural Dynamics*, InTech, 2012. doi: 10.5772/51298.

[3] R. Crowder, "Power transmission and sizing," in *Electric Drives and Electromechanical Systems*, Elsevier, 2020, pp. 73–106. doi: 10.1016/b978-0-08-102884-1.00003-0.

[4] R. Siva Srinivas, R. Tiwari, and C. Kannababu, "Application of active magnetic bearings in flexible rotordynamic systems – A state-of-the-art review," *Mechanical Systems and Signal Processing*, vol. 106. Academic Press, pp. 537–572, Jun. 01, 2018. doi: 10.1016/j.ymssp.2018.01.010.

[5] H. Habermann and G. Liard, "An active magnetic bearing system," *Tribol Int*, vol. 13, no. 2, p. 85, Apr. 1980, doi: 10.1016/0301-679X(80)90021-3.

[6] M. Basso, G. Donati, and M. Mugnaini, "Smart Fault Dictionary for Active Magnetic Bearings Systems," in *2023 IEEE International Workshop on Metrology for Industry 4.0 & IoT (MetroInd4.0&IoT)*, IEEE, Jun. 2023, pp. 360–365. doi: 10.1109/MetroInd4.0IoT57462.2023.10180183.

[7] D. P. Fleming, "Magnetic Bearings-State of the Art," 1991.

[8] K. Gupta Editor, “Symposium on Emerging Trends in Rotor Dynamics.” [Online]. Available: www.springer.com/series/7695

[9] J. Chen, J. Zhu, and E. L. Severson, “Review of Bearingless Motor Technology for Significant Power Applications,” *IEEE Trans Ind Appl*, vol. 56, no. 2, pp. 1377–1388, Mar. 2020, doi: 10.1109/TIA.2019.2963381.

[10] R. Siva Srinivas, R. Tiwari, and C. Kannababu, “Application of active magnetic bearings in flexible rotordynamic systems – A state-of-the-art review,” *Mechanical Systems and Signal Processing*, vol. 106. Academic Press, pp. 537–572, Jun. 01, 2018. doi: 10.1016/j.ymssp.2018.01.010.

[11] A. H. Pesch and J. T. Sawicki, “Active magnetic bearing online levitation recovery through m-Synthesis robust control,” *Actuators*, vol. 6, no. 1, Mar. 2017, doi: 10.3390/act6010002.

[12] Schweitzer G, “Active magnetic bearings-chances and limitations,” Zurich, Oct. 2002. doi: 10.1007/978-3-642-00497-1.

[13] K. Maraiya and Dr. M. Tripathi, “IoT and Its State of Art Applications: A Survey,” *Saudi Journal of Engineering and Technology*, vol. 7, no. 5, pp. 211–217, May 2022, doi: 10.36348/sjet.2022.v07i05.002.

[14] A. Senthil Kumar and E. Iyer, “An industrial iot in engineering and manufacturing industries - Benefits and challenges,” *International Journal of Mechanical and Production*

*Engineering Research and Development*, vol. 9, no. 2, pp. 151–160, Apr. 2019, doi: 10.24247/ijmperdapr201914.

[15] A. Karmakar, N. Dey, T. Baral, M. Chowdhury, and M. Rehan, "Industrial internet of things: A review," in *2019 International Conference on Opto-Electronics and Applied Optics, Optronix 2019*, Institute of Electrical and Electronics Engineers Inc., Mar. 2019. doi: 10.1109/OPTRONIX.2019.8862436.

[16] S. J. Yoo, S. Kim, K. H. Cho, and H. J. Ahn, "Data-Driven Self-sensing Technique for Active Magnetic Bearing," *International Journal of Precision Engineering and Manufacturing*, vol. 22, no. 6, pp. 1031–1038, Jun. 2021, doi: 10.1007/s12541-021-00525-x.

[17] V. E. Balas Vijender, K. Solanki, R. Kumar, and M. Khari, "Intelligent Systems Reference Library 154 Internet of Things and Big Data Analytics for Smart Generation." [Online]. Available: http://www.springer.com/series/8578

[18] D. Jiang and P. Kshirsagar, "Analysis and Control of a Novel Power Electronics Converter for Active Magnetic Bearing Drive," *IEEE Trans Ind Appl*, vol. 53, no. 3, 2017, doi: 10.1109/TIA.2017.2650869.

[19] East China Jiaotong University *et al.*, *Proceedings of the 31st Chinese Control and Decision Conference (2019 CCDC) : 3-5 June, 2019, Nanchang, China*.

[20] W. G. Hurley, M. C. Duffy, J. Acero, Z. Ouyang, and J. Zhang, “Magnetic Circuit Design for Power Electronics,” in *Power Electronics Handbook, Fourth Edition*, Elsevier, 2017, pp. 571–589. doi: 10.1016/B978-0-12-811407-0.00019-2.

[21] Z.-D. Xu, Y.-Q. Guo, J.-T. Zhu, and F.-H. Xu, “Design and Parameters Optimization on Intelligent Control Devices,” in *Intelligent Vibration Control in Civil Engineering Structures*, 2017. doi: 10.1016/b978-0-12-405874-3.00005-9.

[22] L. M. C. Molina, A. Bonfitto, A. Tonoli, and N. Amati, “Identification of Force-Displacement and Force-Current Factors in an Active Magnetic Bearing System,” in *IEEE International Conference on Electro Information Technology*, 2018. doi: 10.1109/EIT.2018.8500155.

[23] S. Y. Yoon, Z. Lin, and P. E. Allaire, *Control of Surge in Centrifugal Compressors by Active Magnetic Bearings*. in Advances in Industrial Control. London: Springer London, 2013. doi: 10.1007/978-1-4471-4240-9.

[24] East China Jiaotong University *et al.*, *Proceedings of the 31st Chinese Control and Decision Conference (2019 CCDC) : 3-5 June, 2019, Nanchang, China*.

[25] N. S. Gibson, H. Choi, and G. D. Buckner, “H∞ control of active magnetic bearings using artificial neural network identification of uncertainty,” in *Proceedings of the IEEE International Conference on Systems, Man and Cybernetics*, 2003. doi: 10.1109/icsmc.2003.1244616.

[26] A. K. Sikder, G. Petracca, H. Aksu, T. Jaeger, and A. S. Uluagac, “A Survey on Sensor-based Threats to Internet-of-Things (IoT) Devices and Applications,” Feb. 2018, [Online]. Available: http://arxiv.org/abs/1802.02041

[27] W. Kassab and K. A. Darabkh, “A–Z survey of Internet of Things: Architectures, protocols, applications, recent advances, future directions and recommendations,” *Journal of Network and Computer Applications*, vol. 163, Aug. 2020, doi: 10.1016/j.jnca.2020.102663.

[28] X. Perry, *Designing Embedded Systems and the Internet of Things (IoT) with the Arm® Mbed™*. 2018. doi: 10.1002/9781119364009.

[29] S. Al-Sarawi, M. Anbar, K. Alieyan, and M. Alzubaidi, “Internet of Things (IoT) communication protocols: Review,” in *ICIT 2017 - 8th International Conference on Information Technology, Proceedings*, 2017. doi: 10.1109/ICITECH.2017.8079928.

[30] B. Stiller, E. Schiller, and C. Schmitt, “An Overview of Network Communication Technologies for IoT.”

[31] R. Herrero, “Textbooks in Telecommunication Engineering Fundamentals of IoT Communication Technologies,” 2020. [Online]. Available: http://www.springer.com/series/13835

[32] H.-K. Chiang, Y.-S. Chang, C.-T. Chu, and T.-J. Chang, “Real Time Bluetooth Human Interface with MSP432 Control in Active Magnetic Bearing System.”

[33] F. Talha, A. Khan, F. A. Shaikh, S. Khan, and M. F. Siddiqui, “Real-Time Wireless Monitoring for Three Phase Motors in Industry: A Cost-Effective Solution using IoT,” 2019.

[34] G. Mamatha and A. H. Thejaswi, “Induction Motor Condition Monitoring and Controlling Based on IoT,” *International Journal of Research in Engineering, Science and Management*, vol. 4, no. 9, pp. 2581–5792, 2021, Accessed: Sep. 13, 2023. [Online]. Available: https://www.ijresm.com

[35] A. H. Pesch and P. N. Scavelli, “Condition monitoring of active magnetic bearings on the Internet of Things,” *Actuators*, vol. 8, no. 1, 2019, doi: 10.3390/act8010017.

[36] X. Li and J. Zhong, “Upper Limb Rehabilitation Robot System Based on Internet of Things Remote Control,” *IEEE Access*, vol. 8, pp. 154461–154470, 2020, doi: 10.1109/ACCESS.2020.3014378.

[37] A. Choudhary, S. Jamwal, D. Goyal, R. K. Dang, and S. Sehgal, “Condition Monitoring of Induction Motor Using Internet of Things (IoT),” in *Lecture Notes in Mechanical Engineering*, Springer Science and Business Media Deutschland GmbH, 2020, pp. 353–365. doi: 10.1007/978-981-15-1071-7_30.

[38] M. Ashmitha, D. Dhanusha, and G. Biju George, “Real Time Monitoring IoT Based Methodology for Fault Detection in Induction Motor,” *Irish Interdisciplinary Journal of Science & Research (IIJSR)*, vol. 5, no. 2, [Online]. Available: www.iijsr.com72

[39] X. Yuan, Y. He, S. Wan, M. Qiu, and H. Jiang, “Remote Vibration Monitoring and Fault Diagnosis System of Synchronous Motor Based on Internet of Things Technology,” *Mobile Information Systems*, vol. 2021, 2021, doi: 10.1155/2021/3456624.

[40] P. IEEE Industrial Electronics Society. Conference (45th : 2019 : Lisbon, Universidade Nova de Lisboa, Institute of Electrical and Electronics Engineers, and IEEE Industrial Electronics Society, *Proceedings, IECON 2019-45th Annual Conference of the IEEE Industrial Electronics Society : Convention Center, Lisbon, Portugal, 14-17 October, 2019*.

[41] D. Meeker, “Finite Element Method Magnetics,” 2015.